Maximizing the Scientific Application of Pandora Column Observations of HCHO and NO_2

Prajjwal Rawat[1], James H. Crawford[1], Katherine R. Travis[1], Laura M. Judd[1], Mary Angelique G. Demetillo[1], Lukas C. Valin[2], James J. Szykman[2], Andrew Whitehill[2], Eric Baumann[2], Thomas F. Hanisco[3]

[1]NASA Langley Research Center, Hampton, VA, 23681, United States
[2]Environmental Protection Agency Office of Research and Development, Research Triangle Park, NC, 27709, US
[3]NASA Goddard Space Flight Center, Greenbelt, MD 20771, USA

Correspondence to: Prajjwal Rawat (prajjwal.rawat@nasa.gov) and James H. Crawford (james.h.crawford@nasa.gov)

Abstract.

As part of the Pandonia Global Network (PGN), Pandora spectrometers are widely deployed around the world. These ground-based, remote-sensing instruments are federated such that they employ a common algorithm and data protocol for reporting on trace gas column densities and lower atmospheric profiles using two modes based on direct-sun and sky-scan observations. To aid users in the analysis of Pandora observations, the PGN standard quality flagging procedure assigns flags to the data indicating high, medium, and low quality. This work assesses the suitability of these data quality flags for filtering data in the scientific analysis of formaldehyde (HCHO) and nitrogen dioxide (NO_2), two critical precursors controlling tropospheric ozone production. Pandora data flagged as high quality assures scientifically valid data and is often more abundant for direct-sun NO_2 columns. For direct-sun HCHO and sky-scan observations of both molecules, large amounts of data flagged as low quality also appear to be valid. Upon closer inspection of the data, independent uncertainty is shown to be a better indicator of data quality than the standard quality flags. After applying a filter on independent uncertainty, Pandora data flagged as medium or low quality in both modes can be demonstrated to be scientifically useful. Demonstrating the utility of this filtering method is enabled by correlating contemporaneous but independent direct-sun and sky-scan observations. When evaluated across 15 Pandora sites in North America, this new filtering method can recover as much as 90% of data that would have previously been discarded. This method suggests that standard PGN criteria for atmospheric variability and normalized root mean squared error are too stringent as they are responsible for downgrading most of the recovered data. A method is also developed for combining the direct-sun and sky-scan observations into a single dataset by accounting for biases between the two observing modes and differences in measurement integration times. This combined data provides a more

continuous record useful for interpreting Pandora observations against other independent variables such as hourly observations of surface ozone. When Pandora HCHO columns are correlated with surface ozone measurements, data filtered by independent uncertainty exhibits similarly strong and more robust relationships than high-quality data alone. These results suggest that Pandora data users should carefully assess data across all quality flags and consider their potential for useful application to scientific analysis. The present study provides a method for maximizing use of Pandora data with expectation of more robust satellite validation and comparisons with ground-based observations in support of air quality studies.

1 Introduction

The Pandora spectrometer is a ground-based UV-visible (UV-VIS) remote-sensing instrument utilized to validate space-based UV-VIS sensors and understand local air quality (Herman et al., 2009; Wang et al., 2010; Spinei et al., 2018; Tzortziou et al., 2012; Herman et al., 2019; Szykman et al., 2019; Judd et al., 2019; Verhoelst et al., 2021; Di Bernardino et al., 2023). The Pandora instrument was developed to observe column nitrogen dioxide (NO_2) in direct-sun mode, in addition to the more traditional sky-scan observations obtained using multi axis differential optical absorption spectroscopy (MAX-DOAS). Once calibrated, direct-sun observations are less impacted by atmospheric parameters that influence the air mass factor (AMF) and which also cause uncertainty in space-based retrievals, such as the vertical gas profile or surface albedo (Cede et al., 2006; Herman et al., 2009). More recently, Pandora instrument retrievals of column formaldehyde (HCHO) have become available, expanding opportunities to evaluate the importance of both nitrogen oxides (NO_x) and volatile organic compounds (VOCs) as precursors of ozone and secondary aerosol. This was enabled by the removal of instrument components made of Delrin which were discovered to outgas HCHO and interfere in its detection (Spinei et al., 2021).

The Pandonia Global Network (PGN) is a NASA and ESA-sponsored ground-based network of Pandora spectrometers supporting in situ and remotely sensed air quality monitoring and satellite validation activities (https://www.pandonia-global-network.org). The major advantages of the PGN are uniform instrument design, homogeneous calibrations, centralized data monitoring and processing, and real-time data distribution (Herman et al., 2009, 2018; Spinei et al., 2018; Herman et al., 2019; Cede et al., ~~2021~~2024). Pandora instruments are calibrated by NASA Goddard Space

Flight Center and deployed to local operators around the world who join the PGN. Consistent retrievals across the network are performed by LuftBlick Earth Observation Technologies and are hosted on the PGN website (Cede et al., ~~2021~~2024). Presently, there are more than 130 Pandora instruments worldwide and over 60 across the U.S. (Szykman et al., 2019; Chang et al., 2022).

Pandora instruments have provided valuable information on NO_2 retrieval biases from the polar-orbiting Sentinel-5P TROPOspheric Monitoring Instrument (TROPOMI) (Judd et al., 2020; Verhoelst et al., 2021; Park et al., 2022; Ialongo et al., 2020) and Ozone Monitoring Instrument (OMI) (Tzortziou et al., 2012; Reed et al., 2015; Herman et al., 2019). The high temporal availability of Pandora data has allowed for deep investigation of local meteorology on column NO_2 and how well that is captured by air quality models (Goldberg et al., 2017; Choi et al., 2020; Tzortziou et al., 2022; Wang et al., 2023; Adams et al., 2023; Tzortziou et al., 2023). The relatively new formaldehyde retrievals from Pandora (Spinei et al., 2018, 2021; Cede et al., ~~2023a~~2025) are beginning to be incorporated into model and satellite validation efforts (Herman et al., 2018) and show promise for characterizing the local ozone photochemical environment (Schroeder et al., 2016; Travis et al., 2022).

Geostationary satellite observations provide a new challenge in interpreting NO_2 and HCHO columns at unprecedented spatial and temporal scales (Kim et al., 2017; Judd et al., 2018). Pandora instruments will be the main source of validation data for both NO_2 and HCHO columns for the Tropospheric Emissions: Monitoring of Pollution (TEMPO) geostationary air quality satellite launched over the U.S. in 2023 (Szykman and Liu, 2023; Zoogman et al., 2017). Pandora instruments are also being used to validate the Geostationary Environmental Monitoring Spectrometer (GEMS) satellite retrievals over East Asia (Kim et al., 2023). Given the growing need for Pandora data to support satellite observations and model development, improved methods for ensuring data availability and quality are needed. In this work, a data filtering method is presented for assessing suitability of HCHO and NO_2 column data beyond the standard quality flags provided by PGN. This method takes advantage of the independent but contemporaneous measurement modes of Pandora operation (direct-sun and sky-scan) to analyze Pandora data quality and maximize the availability of data for scientific application. The method presented here is but one approach to examine Pandora data quality. The user community should continue to carefully consider how to best ensure data quality while preserving the most data possible.

2 Data and methodology

2.1 Pandora measurements and data retrieval

The Pandora spectrometer is an instrument for ground-based remote sensing of a range of trace gases, including NO_2, HCHO, O_3, and SO_2, with temporal resolution on the order of seconds to minutes. Pandora is a passive UV-VIS spectrometer system equipped with a responsive sun tracker that points the optical head sensor to the sun or sky with a spatial accuracy of up to ±0.1°. A basic description of the Pandora instrument is summarized here with additional details provided in supplementary section S1.1 and available in Cede et al. (~~2021~~2024). Briefly, light is transmitted through fiber optical cables to a UV-VIS low stray light spectrometer (Herman et al., 2009; Tzortziou et al., 2012). The spectrometer covers a spectral range of 280-530 nm with a spectral resolution of 0.6 nm. To minimize the dark current noise, the spectrometer is maintained at a stable temperature of 15-20°C (based on the site location) using a thermal electrical cooler. The Pandora spectrometer operates in two daytime viewing geometries, namely, direct-sun (DS) and scattered sunlight or sky-scan (SS) (Figure 1), with varying degrees of temporal resolution spanning from milliseconds to minutes depending on the mode of operation.

The Pandora retrieval involves several sequential steps or data processing levels that are all archived by PGN. Raw measurement spectra are archived as L0. L1 data include corrections for instrumental characteristics such as dark signal, non-linearity, flat field, temperature sensitivity, simple stray light removal, and wavelength corrections. L2Fit data includes spectral fitting, which enables calculation of slant column amounts relative to the reference spectrum employing DOAS analysis (Herman et al., 2009; Cede, 2022; Gebetsberger et al., ~~2023a~~2023). L2 data results from the conversion of slant columns to vertical columns utilizing geometrical AMFs for direct-sun and analytical methods for sky-scan observations. Sky-scan observations also include profile and surface concentrations. These products are briefly described in the supplement to this paper (section S1.1). The reported accuracy of the DS total vertical column of NO_2 is 2.7×10^{15} molecules cm^{-2} (0.1 Dobson unit, where 1 DU = 2.7×10^{16} molecules cm^{-2}) with a precision of 2.7×10^{14} molecules cm^{-2} (0.01 DU) (Herman et al., 2009). For HCHO DS a small statistical error up to 6% and notable systematic error up to 26% have been reported (Spinei et al., 2018, 2021) while the

recent Pandora Delrin-free instruments require more assessment for quantifying accuracy and precision. The Pandora SS measurements still lack a robust validation; however, the CINDI-2 intercomparison included a Pandora (named as NASA instrument) and reported a bias for measurements in the SS mode of about -0.05×10^{16} molecules cm^{-2} for HCHO column and about -0.02×10^{16} molecules cm^{-2} for NO_2 column against the median of the participating instruments (Tirpitz et al., 2021; Verhoelst et al., 2021). Additional details on current Pandora software, recent hardware changes, and retrieval scheme are discussed in supplementary section S1.1.

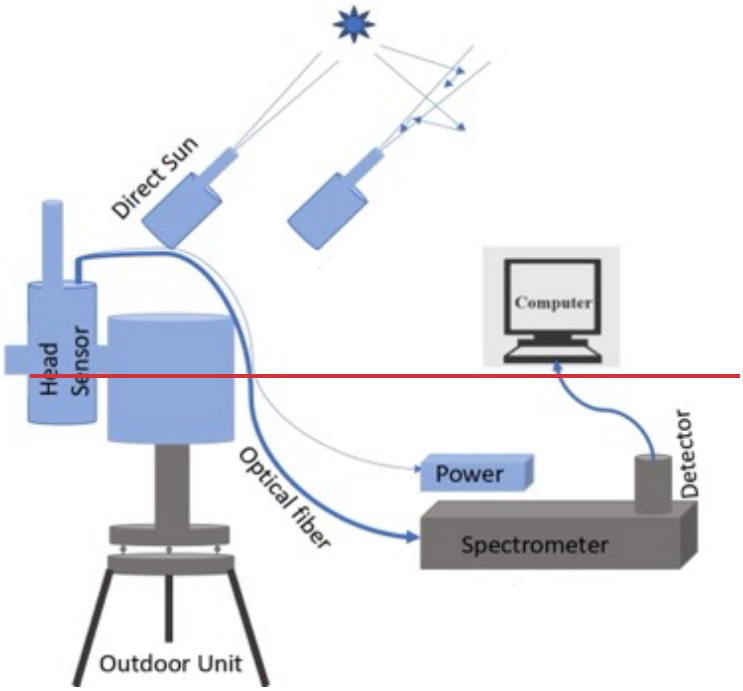

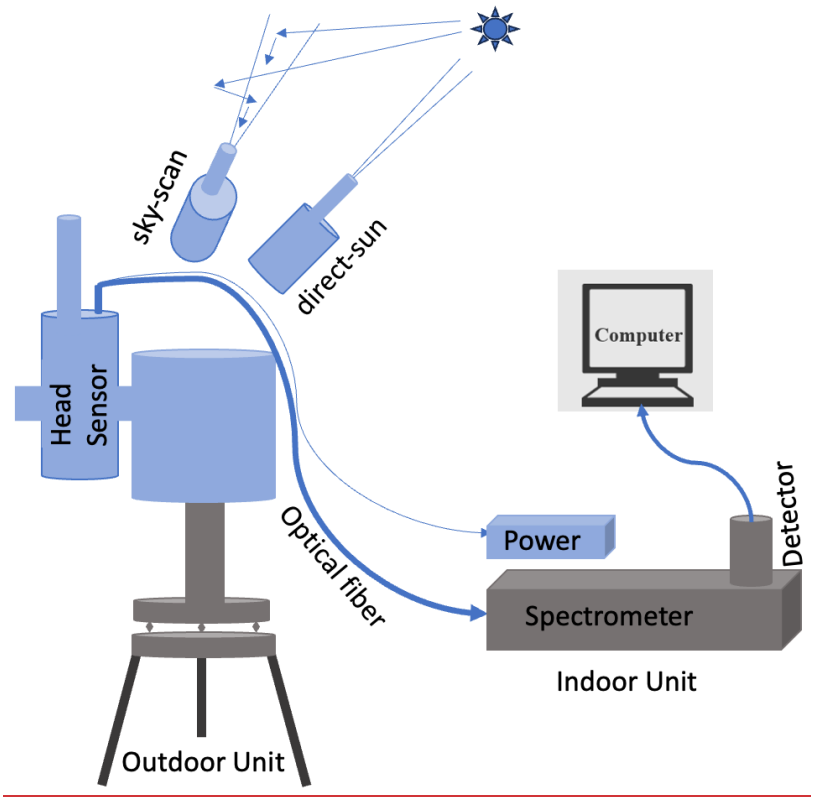

Figure 1. Block diagram of a Pandora instrument and its two viewing geometries.

135

2.2 Pandora observational schedule

Pandora instruments are locally operated and mainly run on the standard schedule alternating between DS and SS mode, although there is an option for user-defined schedules. The DS and SS
140 modes also alternate between an Open (unfiltered) mode for NO_2 and a U340 (filtered for maximum transmission near 340nm) mode for HCHO observations (Cede et al., ~~2021~~2024; Spinei et al., 2018). A typical example of the Pandora standard schedule on a clear sky day is shown in Figure 2a, with the typical total hours per day for each routine annotated. Typically, Pandora spends about 1.5 hrs each day in DS NO_2 (SQ) and DS HCHO (SS, not to be confused with "sky-
145 scan") modes and about 1.5 hrs each in SS mode for lower tropospheric columns of NO_2 and HCHO (EO) and HCHO only (EU). Longer more detailed sky scanning (EL and EK) occurs for a total of about 1-2 hrs for profile observations. Find Sun (FS) routines occur throughout the day, but only take a short time (few seconds) over each hour. Typically, Pandora spends 65% of the

time in SS mode and 30% in DS mode under clear sky conditions. Further details of all Pandora routine acronyms are described in supplementary section S1.2 and the Pandora user manual (Cede et al., ~~2021~~2024). The inset panels in Figure 2 (b and c) provide a closer view of the schedule for an 18-minute window as the instrument switches between DS and SS modes. The varying effective measurement times (t_{eff}) illustrate the observation frequency for each mode and product. Generally, the Pandora instrument possesses the capability to capture solar spectra at adjustable integration times, ranging from 2.5 ms to 4 s, with an overall measurement duration of approximately 40 s, encompassing a few dark current measurements (Cede et al., ~~2021~~2024). The integration time for DS NO_2 (with no filter) under bright sun is about 4 ms, and roughly 4000 spectra are acquired repeatedly and averaged to obtain very high signal-to-noise ratios with high precision (Herman et al., 2018). For DS HCHO (with U340 filter), a longer integration time (30-1000 ms) is used; hence, there are fewer measurements for HCHO compared to NO_2. Typically, in the DS mode, there are about 5 times more observations of NO_2 compared to HCHO column per scan (Figure 2c). In the SS mode, ~~zenith measurement~~elevation scans are ~~routinely collected at specified~~most effective when taken along an azimuth ~~angles, with~~pointing away from the ~~north or 0° being~~sun to minimize the ~~preferred direction for northern hemispherical sites.~~effect of scattering. The zenith angle scans can vary by site with the lowest scan typically occurring between 89° and 85° depending on viewing conditions available at the site to the highest zenith angle (0°), which is utilized as the reference during the spectral fitting (details of different zenith angles are provided in section S1.2). The extended SS measurements are taken at multiple zenith angles (section S1.2) to derive lower tropospheric columns and profiles typically up to 2-4 km.

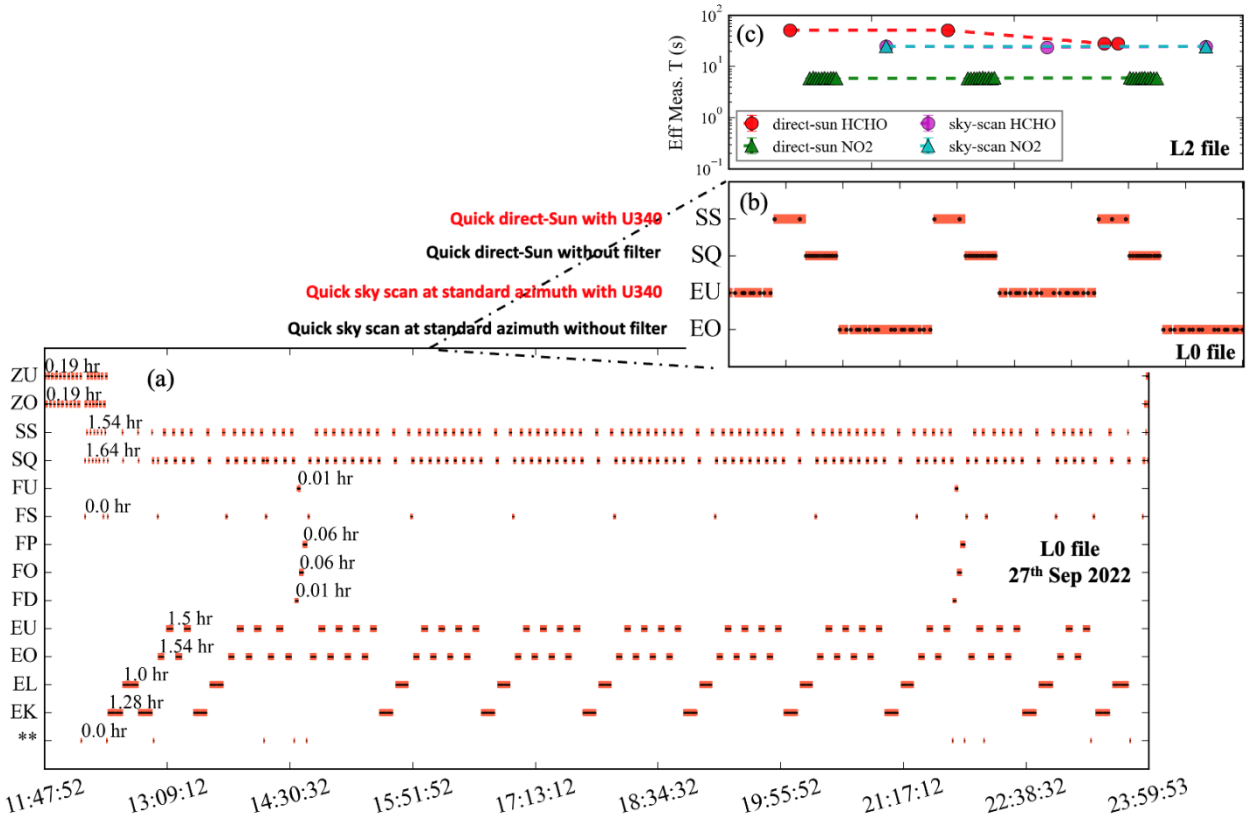

Figure 2. (a) Pandora standard schedule of operations (UTC hour) on a clear sky day on 27 Sep 2022 at the University of Houston site for different observing modes with a zoomed-in, 18-minute window for both L0 (b) and L2 (c) file information. The black points in the L0 schedule show the start of each measurement time and underlying red line is the total time in that respective mode. The L2 data (c) shows the alternating retrieval of NO_2 (without filter) and HCHO (with U340 filter) column from direct-sun and sky-scan modes.

3.0 Pandora data quality flags and an alternative data filtering method

The PGN software suite performs retrievals for NO_2 and HCHO and provides a measure of data quality to guide users (Cede et al., ~~2021, 2023a, 2023b).~~2024, 2025). Reduced data quality can arise from instrumental and/or atmospheric sources. Data flags provide information on both the data quality and data assurance level (Gebetsberger et al., ~~2023b~~2022). Data quality is indicated in the units position, with a 0, 1, or 2 indicating high, medium, and low quality respectively. While data that is preliminary, but not yet quality assured, is useable for science, this status is indicated by a 1 in the tens position. Data that is unusable for whatever reason are indicated by a 2 in the tens position. Thus, data flagged as 0 or 10 are considered useable and high quality, and users are cautioned to pay additional scrutiny to data flagged as 1 or 11 (medium quality). By contrast, users

are discouraged from using any data flagged as 2 or 12 (low quality). These quality flags are assigned in various stages from L1 (raw data) to L2fit (spectral fit data) to L2 (processed data) for ensuring data quality through multiple checks at each stage. At the L1 stage, data is flagged into either low- or medium-quality based on instrument-related issues such as excessive dark counts, detector saturation, dark count differs significantly from the dark map for too many pixels, different effective temperature, and unsuccessful dark background fitting. In the L2fit stage, where spectral fitting is performed, data is further flagged based on factors including the quality of the fit, the wrms limit (normalized rms of fitting residuals weighted with independent uncertainty), and wavelength shift. Finally, at the final retrieval L2 stage, factors including retrieval error and atmospheric variability are used to flag data into the medium or low-quality. More description of the data quality flags is provided in Gebetsberger et al., (~~2023b~~2022).

Following the suggestion of the Pandora user manual (Cede et al., ~~2021, 2023a, 2023b~~2024, 2025), many previous studies with Pandora v1.8 data utilize only high-quality data (0, 10) (e.g., Park et al., 2022; Verhoelst et al., 2021; Liu et al., 2023). However, when using only high-quality flagged data, a large fraction of observations is often eliminated. Figure 3 shows quality flag statistics across the 15 Pandora sites evaluated in this study (listed in Table S1). They have been selected since they fall under recent NASA airborne campaigns that covered areas of the eastern U.S. and Houston, TX. These are the Tracking Aerosol Convection Interactions Experiment-Air Quality (TRACER-AQ) in 2021, the Student Airborne Research Program (SARP-East) in 2023, and the Synergistic TEMPO Air Quality Science (STAQS) study in 2023. Across these sites, high-quality data flags dominate only for DS NO_2 observations during the 2021-2022 period, typically being between 60-80%. For other observations, low quality data flags often dominate, on average accounting for 57%, 45%, and 46% of data for SS NO_2, DS HCHO, and SS HCHO, respectively, across the evaluated sites, making much of the data unavailable for supporting field campaign analysis.

The schedule of Pandora operations shown in Figure 2 demonstrates the contemporaneous nature of DS and SS observations. Figure 3 further shows that the quality flags for the two observing methods can often differ substantially. This enables an independent assessment of data quality by taking advantage of the expected autocorrelation of contemporaneous (within 5 min) DS and SS observations for different quality flag combinations. An example is provided in Figure 4 showing

HCHO observations for the University of Houston Pandora site. Note that there are nine possible combinations of high, medium, and low-quality data pairs. More than half of those data pairs (57%) include one low-quality observation. Low-quality SS observations correlate as well or better with medium and high-quality data as do data pairings including only medium and high-quality data. There is more scatter in the data that include low-quality DS observations (right column of panels in Figure 4), but there is still evidence of a large number of well correlated data, even for pairings of low-quality data for both DS and SS modes. Given the independent nature of the DS and SS observations, it is worthwhile to examine the role of measurement uncertainty in these correlations.

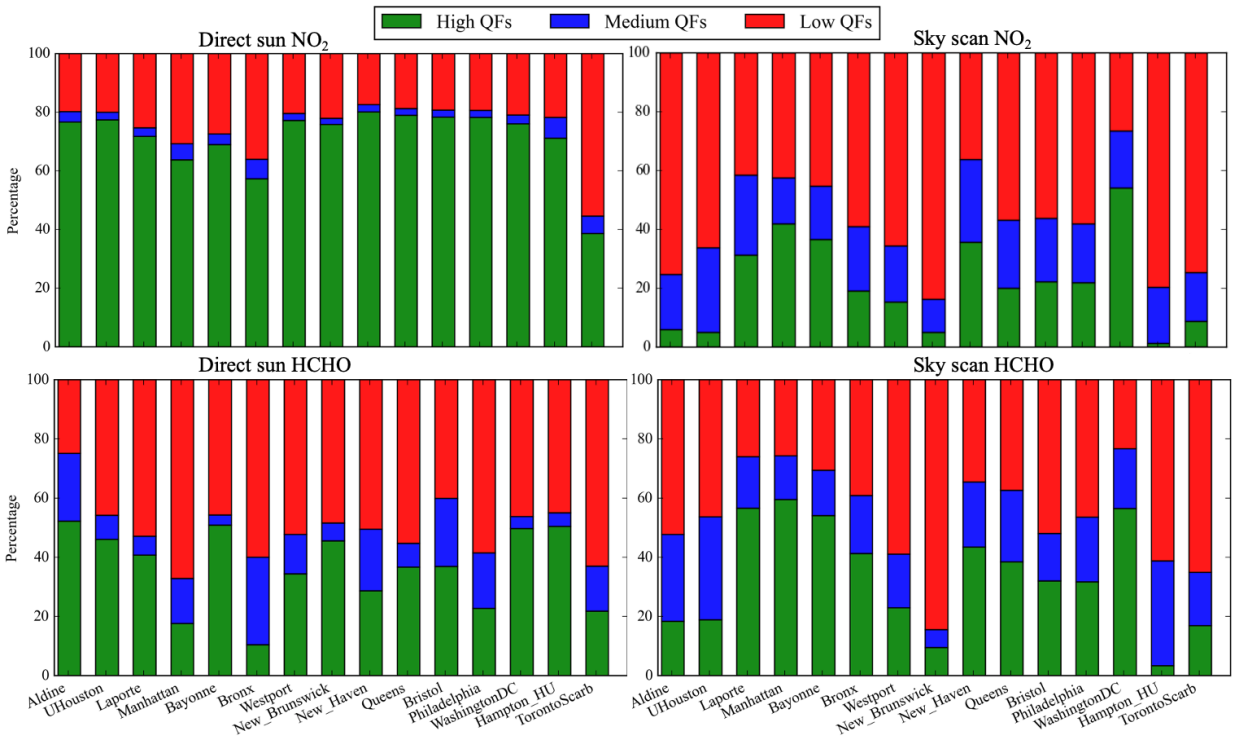

Figure 3. Percentage contribution of high (0, 10), medium (1, 11), and low (2, 12) quality flags for 15 Pandora sites for observations in both DS (left panels) and SS (right panels) modes during 2021-2022. Percentage contributions are shown for NO_2 in the top panels and HCHO in the bottom panels.

Figure 5 shows the frequency distribution of independent uncertainty for high, medium, and low-quality Pandora HCHO and NO_2 column observations for both DS and SS mode for non-negative vertical columns at the University of Houston Pandora site. Independent uncertainty is a measure

of the photon noise across the detector pixels which is propagated to slant columns for each retrieval and provided in the L2 product. Figure 5 shows that there is significant overlap in the independent uncertainty distribution across all three quality flags for each measurement mode. The figure inset shows the corresponding cumulative probability distributions and cut-off value (black dotted line) that preserves almost all high-quality data while including a significant amount of overlapping data flagged as medium or low quality. In the present analysis, the cut-off value for independent uncertainty is defined as $\mu + 3\sigma$ of the independent uncertainty distribution for high-quality data, where μ is mean and σ is standard deviation. The gray shaded area in Figure 5 shows the portion of the data falling outside this limit. For the University of Houston Pandora, the cut-off values are 0.37×10^{15} molecules cm^{-2} for DS independent uncertainty and 1.79×10^{15} molecules cm^{-2} for SS independent uncertainty in HCHO column measurements. For NO_2 column measurements the cut-off values are 0.62×10^{14} molecules cm^{-2} for DS independent uncertainty and 1.81×10^{14} molecules cm^{-2} for SS independent uncertainty. In this method, Pandora data having independent uncertainty less than the cut-off limit are further scrutinized for scientific utility regardless of their data flag.

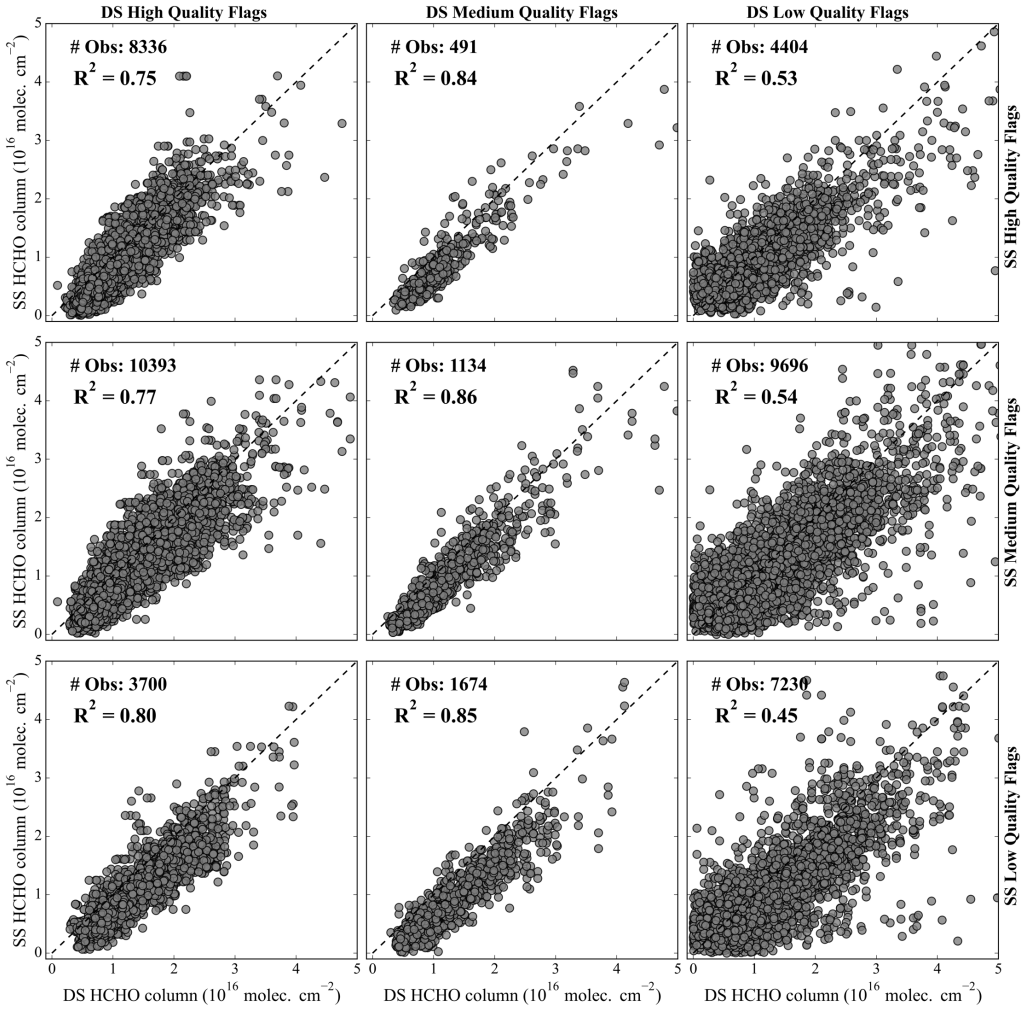

255

Figure 4. Correlation of contemporaneous DS and SS observations of HCHO column for different quality flag combinations. Data is from the University of Houston Pandora site over two years (2021-2022).

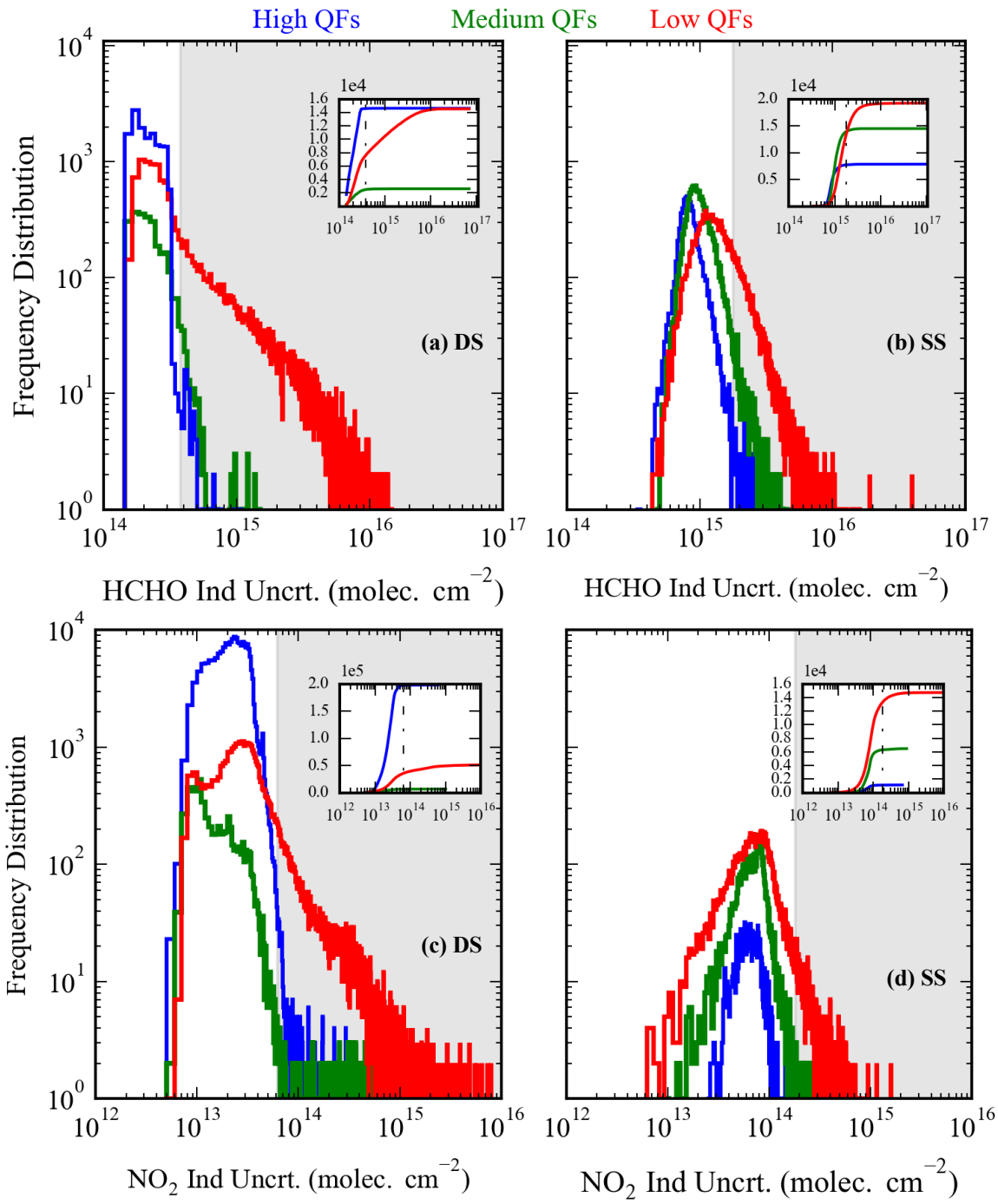

Figure 5. Frequency distribution of independent uncertainty in three quality flags: high (blue), medium (green) and low (red) for a) column HCHO direct-sun, b) column HCHO sky-scan, c) column NO_2 direct-sun, and d) column NO_2 sky-scan observations at the University of Houston Pandora site. The cumulative distributions for each panel are inset with the cut-off values used in the present analysis shown as a black dashed vertical line. Data values exceeding the cut-off are shaded in gray for the frequency distributions.

This proposed data filtering method is evaluated in Figure 6 for HCHO observations at the University of Houston Pandora site, showing how specific data pairs are related to the independent uncertainty cut-off values. Data pairs with uncertainty falling above the cut-off for DS only (blue points) and both DS and SS (red) are almost exclusively limited to the low-quality flagged data (right column and bottom row of panels in Figure 6). These points also account for most of the scatter in the correlations. Data pairs with uncertainty falling above the cut-off for SS data only (yellow) tend toward larger column amounts. This calls for a second filtering step in which observations with independent uncertainties of less than 10% of the column amount are retained even if the absolute independent uncertainty exceeds the cut-off value. This preserves a small but important set of large column abundances that are important for exploring the full dynamic range of column variability.

Finally, there can be a few rare outliers (< 0.1%) associated with unusually large wrms values even after applying this independent uncertainty cut-off. For this analysis, we empirically determine that these outliers are associated with unusually high values for DS and SS data of high wrms and for SS data of maximum horizontal distance (MHzD). These outliers can be removed with thresholds for wrms of 0.01 and MHzD of 20km. Specific column numbers from Pandora files for the variables used in this analysis are provided in Table S2 to facilitate application of this method.

Figure 7 shows the filtered data for the University of Houston Pandora site colored by data density. After the filtering method is applied, correlations notably improve for combinations that include DS low quality flagged data. Among all pairings (R^2 = 0.72 to 0.86), data quality flags no longer appear to be a useful predictor of correlation between contemporaneous SS and DS observations. This suggests that all remaining data may be scientifically useful regardless of quality flag. Figure 7 also shows that there is a bias between SS and DS observations for HCHO column. This is not unexpected given that SS observations are limited to the lower troposphere, but as discussed later in section 3.3, this bias must be addressed for applications where it is advantageous to combine SS and DS observations into a larger unified data set.

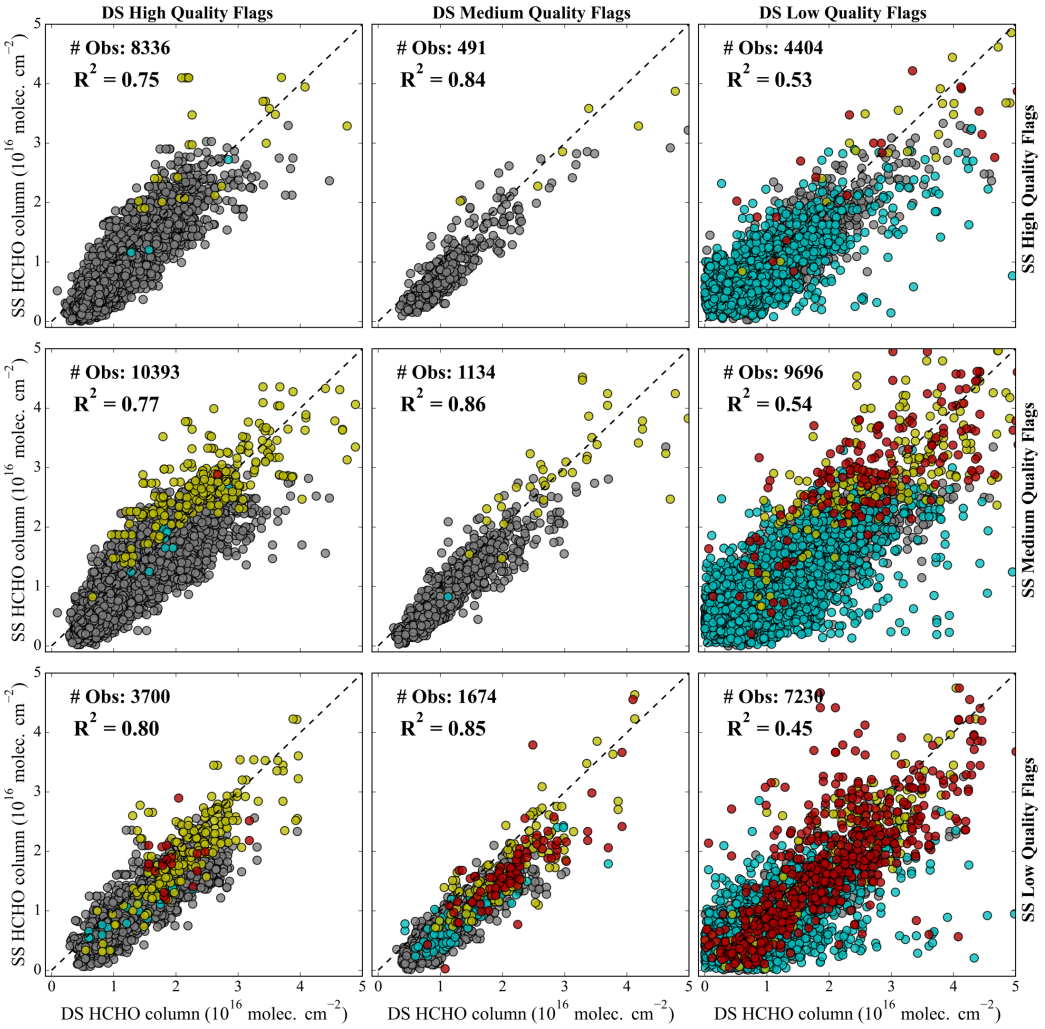

Figure 6. Correlation of contemporaneous DS and SS observations of HCHO column for different quality flag combinations at the University of Houston Pandora site over two years (2021-2022). Data points are colored by cutoff values used for HCHO column independent uncertainty values. Gray indicates points for which both DS and SS uncertainties are less than the cut-off, other colors indicate points for which only DS (cyan), only the SS (yellow), or both DS and SS (red) uncertainties exceed the cut-off value.

Figure 8 shows the same plot as Figure 6 but for NO_2 columns at the University of Houston Pandora site. There are more total pairs in this comparison since DS NO_2 observations are more frequent than HCHO (see Figure 2). Again, reasonable correlation is observed in all the quality flags (R^2 = 0.68 to 0.73). For NO_2, the filtering method leads to very little data being removed, thus correlations are essentially unchanged in Figure 9 for the filtered data. Again, there is a bias with DS values being greater than SS values. This is mainly due to stratospheric NO_2 which is only detected in the DS mode (see discussion in section 3.3). Figures 8 and 9 show that for NO_2,

the frequent DS retrievals enable multiple DS measurements to be matched with a single SS observation within the 5-minute matching window.

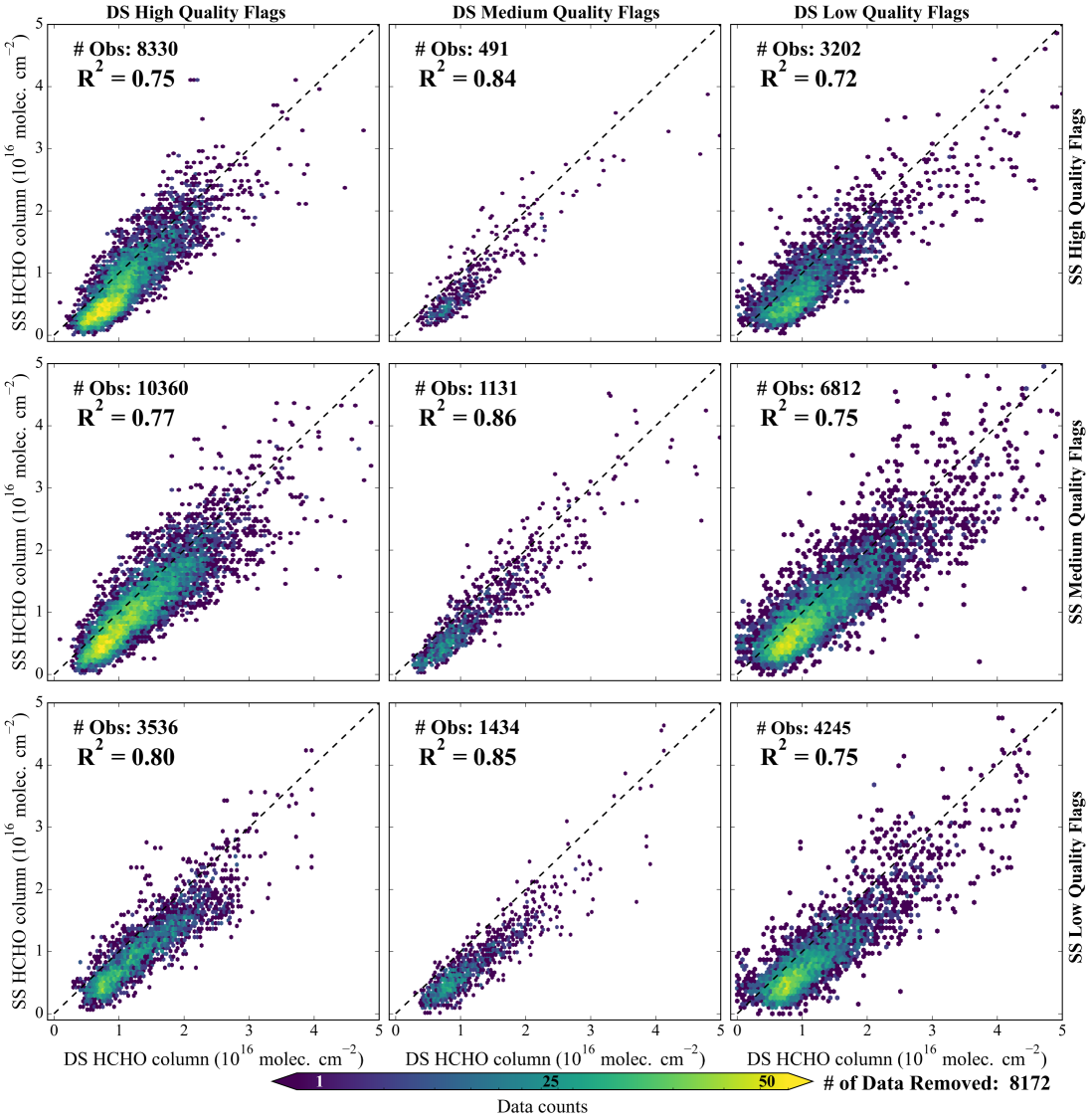

315 **Figure 7.** Correlation of contemporaneous DS and SS observations of HCHO column for different quality flag combinations after applying new filtering method to the University of Houston Pandora site for 2021-2022. Data points are colored ~~by normalized gaussian kernel density of data.~~based on the count within each hexagonal bin (grid size of 100).

320

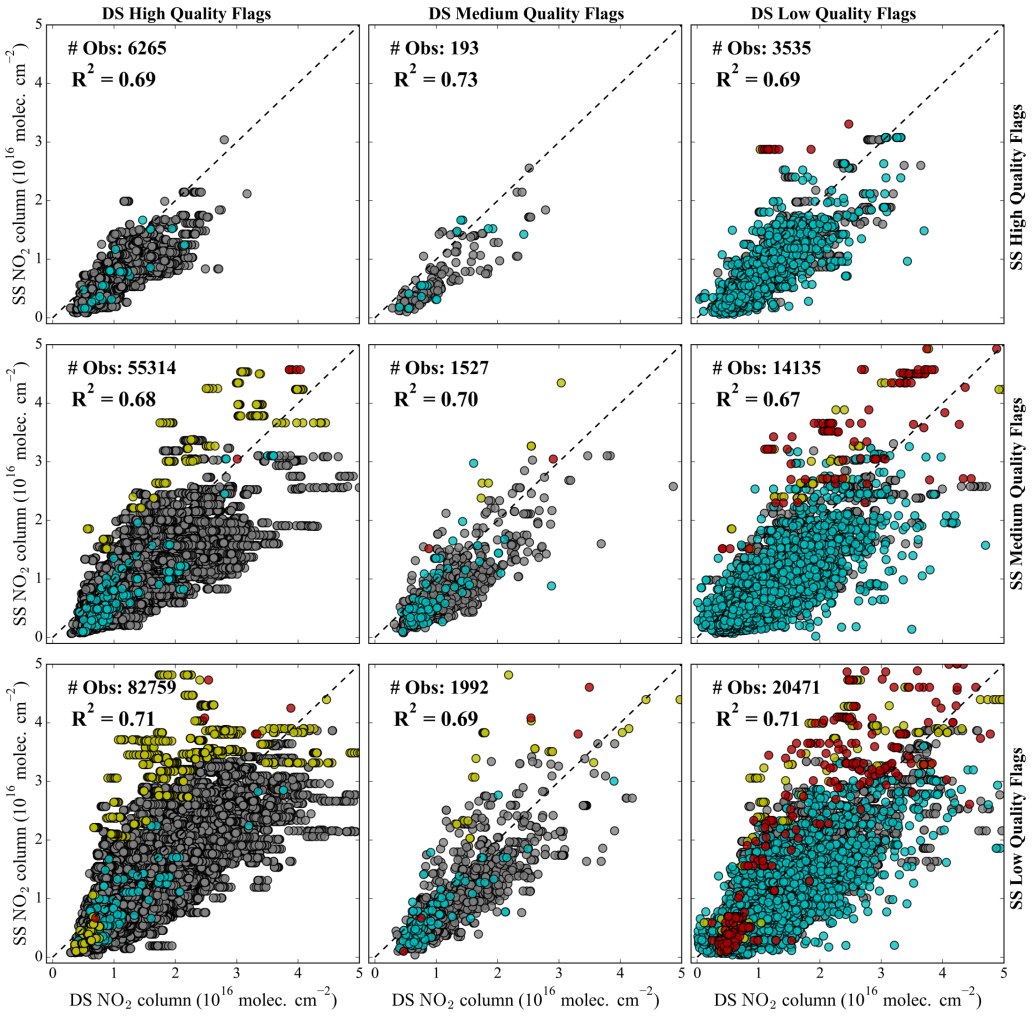

Figure 8. Correlation of contemporaneous DS and SS observations of NO_2 column for different quality flag combinations at the University of Houston Pandora site for 2021—2022. Data points are colored by cutoff values used for NO_2 column independent uncertainty values. Gray indicates points for which both DS and SS uncertainties are less than the cut-off, other colors indicate points for which only DS (cyan), only the SS (yellow), or both DS and SS (red) uncertainties exceed the cut-off value.

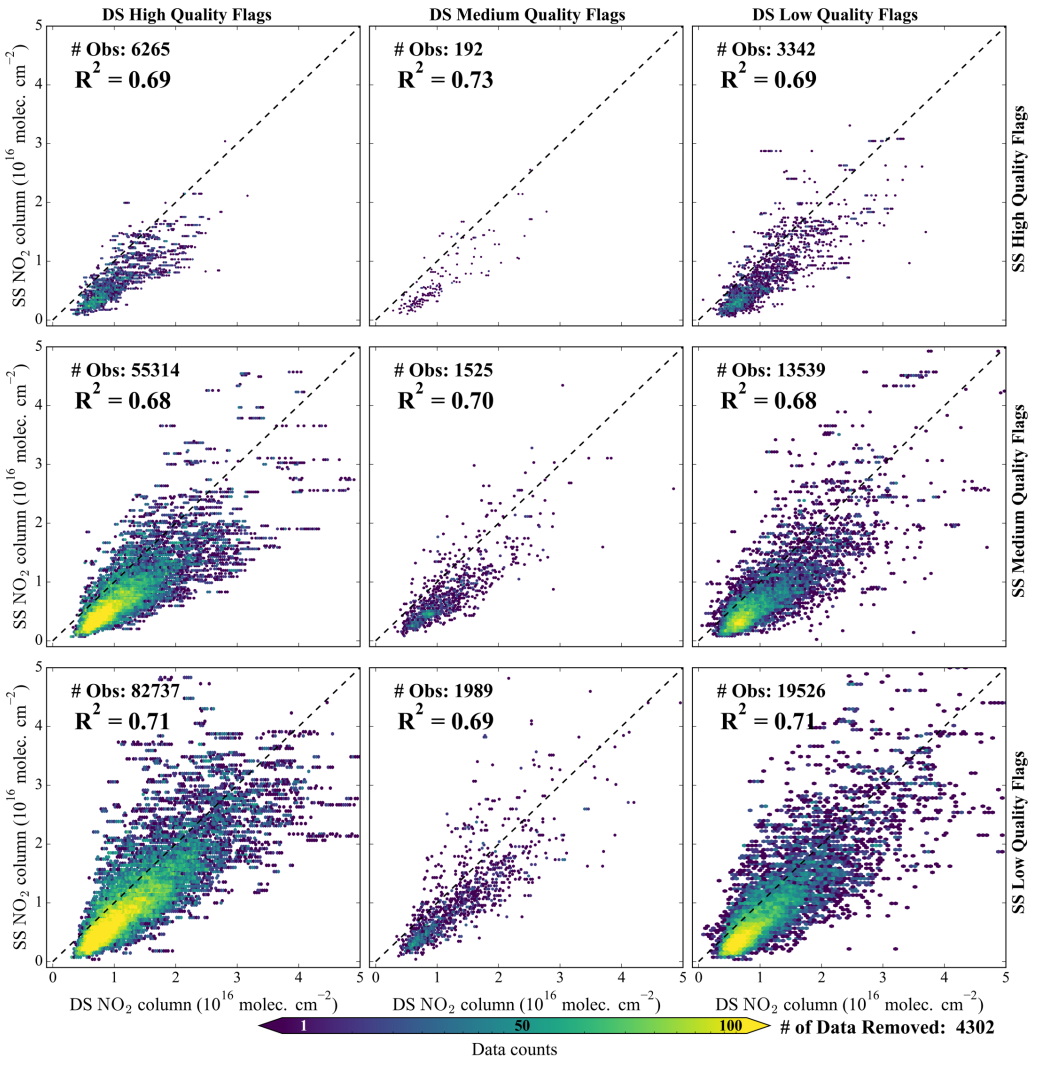

Figure 9. Correlation of contemporaneous DS and SS observations of NO_2 column for different quality flag combinations after applying new filtering method to the University of Houston Pandora site for 2021-2022. Data points are colored ~~by normalized gaussian kernel density of data.~~based on the count within each hexagonal bin (grid size of 150).

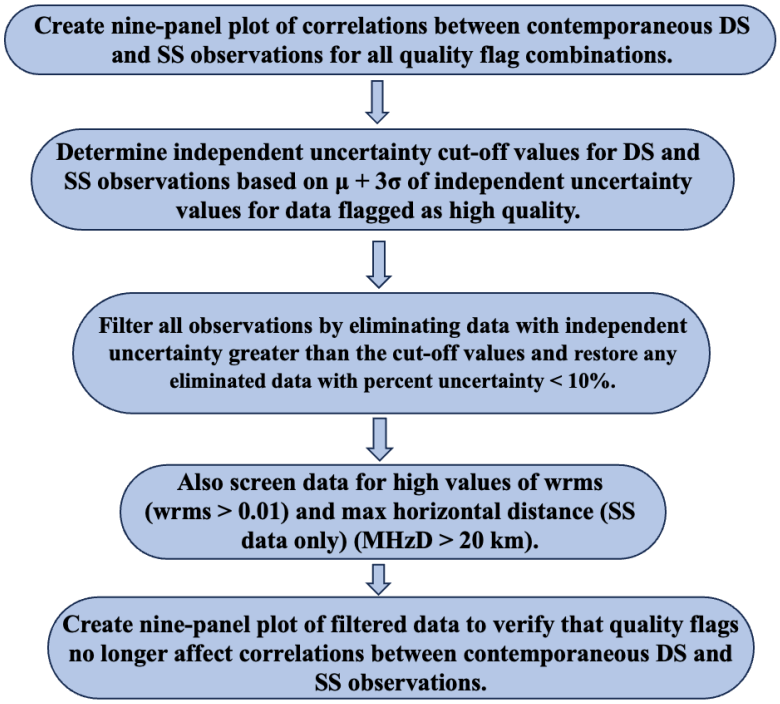

Figure 10. New data filtering method used in the present analysis to increase the scientific availability of Pandora observations.

The method demonstrated in Figures 4 through 9 is summarized in Figure 10. It can be applied to any PGN site with contemporaneous DS and SS observations. Results of applying the method are show in Figure 11 for the 15 Pandora sites falling under recent NASA airborne campaigns. Data from 2021 and 2022 are used for all sites, although La Porte, Texas only has data from August 2021 to February 2022. The bars in Figure 11 show the occurrences of the high (green), medium (blue), and low (red) quality flagged data across these 15 Pandora sites. The amount of available data varies considerably between sites. This can be due to a number of reasons including instrument down time, use of non-standard observing schedules, and periods of data flagged as unusable (20, 21, or 22). The grey bars show the amount of usable data after applying the new filtering method. For HCHO data, 35% is high quality on average. This increases to 77% on average when the new method is applied. For NO_2, this improvement is from 46% to 97%.

In Supplementary Section 1.3, data quality flags are traced for the University of Houston Pandora dataset used in Figures 6 through 9. For DS HCHO, most data are flagged as medium or low quality primarily due to violating the data quality indicators (DQ) for atmospheric variability. Data is also flagged due to high wrms and saturated data. The data recovery procedure shown in Figure 10 restores 34% of data flagged for high wrms and 70% of data flagged for high atmospheric

variability. The large atmospheric variability values are assumed to be related to cloudiness. However, there appears to be no correspondence between atmospheric variability values and actual sky conditions (Figure S1). For SS HCHO, flagging primarily occurs due to saturation or dark count issues in the L1 stage and high wrms in the L2fit stage. Unlike DS measurements, atmospheric variability is rarely triggered for sky-scan HCHO despite observations showing a tendency for greater atmospheric variability. Of the flagged data, 75% of saturated or dark count-affected data and 70% of high wrms-flagged data are recovered. For NO_2, DS data are primarily flagged for exceeding atmospheric variability thresholds, while SS data are flagged for high wrms values. This analysis suggests that the PGN criteria for atmospheric variability, wrms, dark counts, and saturated data may be overly stringent. Of these PGN criteria, wrms is the only one considered in the method outlined in Figure 10, but the threshold value is empirically determined independent of the flagging. Data users are encouraged to continue to pay attention to the impact of wrms on Pandora data quality for specific instruments.

As noted in Figure 10, the first step in verifying the success of the method is to demonstrate the quality of correlation across all quality flag combinations. To further strengthen the case for using this method, independent observations are used in the following sections to demonstrate more robust scientific analyses. Evaluation of biases between DS and SS observations and prospects for combining them into a single data set are also explored.

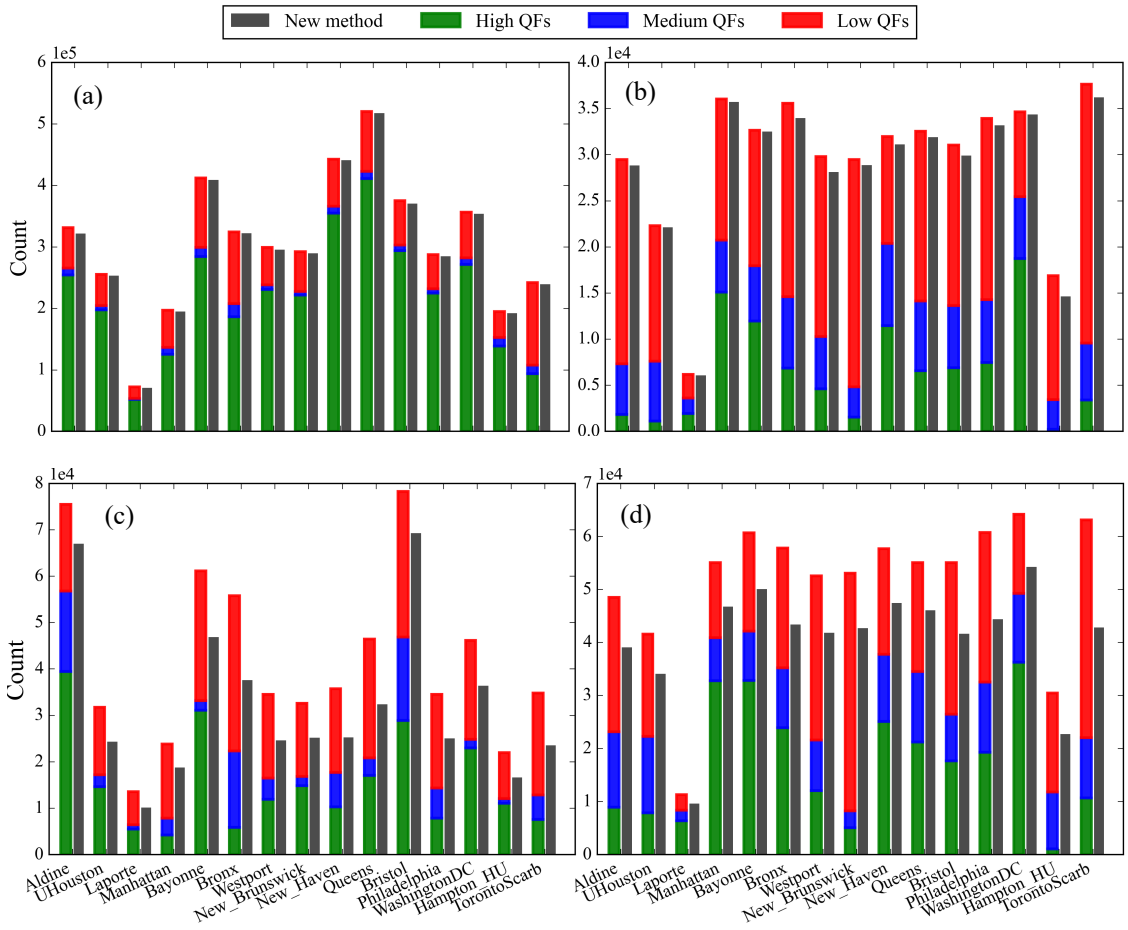

Figure 11. Quality flags (QFs) for each Pandora site in 2021-2022 (left bars) colored by green (high), blue (medium), and red (low) for (a) NO_2 DS, (b) NO_2 SS, (c) HCHO DS, and (d) HCHO SS. Adjacent grey bars show total observation counts after applying the new filtering method.

3.1 Independent assessment of Pandora scientific data quality with HCHO:O_3 analysis

Recent work has shown a strong correlation between surface O_3 and column HCHO (Schroeder et al., 2016; Travis et al., 2022). This relationship is used here to test the effectiveness of the new filtering method on Pandora HCHO column observations for the University of Houston Pandora site during the TRACER-AQ period (September 2021). High-resolution (5-min) collocated surface ozone measurements were obtained from the Texas Commission on Environmental Quality. The Pandora HCHO column measurements in SS and DS modes are temporally matched (within 5 minutes) with surface ozone data between 10:00 and 18:00 local time when photochemistry is most

active. This analysis compares results using only high-quality flagged Pandora data with results using Pandora data filtered with the new method.

Figure 12 shows the relationship between the HCHO column and surface ozone using DS and SS observations. When the new filtering method is applied, the ~~R^2 substantially increased in SS mode from 0.42 (Figure 12a) to 0.57 (Figure 12c) with a five-fold increase in the~~ number of data points increasing by five-fold for SS (181 to 955~~). In DS mode, R^2 remained the same (Figure 12b)~~ and ~~12d) but with over a~~ two-fold for DS (275 to 696). In both cases, the R^2 remains similar or improves. However, the substantial increase in data ~~(275 to 696).~~ density will lead to more robust scientific analysis of the HCHO:O_3 relationship. Similar ~~improvements in correlation and data quantity~~results are obtained for other months outside the TRACER-AQ period that are not shown here.

This analysis is expanded in Table 1 to include Pandora sites that are located within 500 m of an EPA regulatory monitor reporting hourly ozone. Data is for the month of September 2022 which had the best data availability. Table 1 summarizes the resulting correlation between hourly averaged column HCHO in SS and DS modes with hourly surface ozone. Generally, similar or improved correlation and increased data availability (14 – 163%) were observed after applying the new filtering method. However, over the New Brunswick site in DS mode, a lower correlation (0.60 to 0.52) was observed after applying the new method. This was caused by the new method capturing an ozone event (>60 ppb) that appeared to be decoupled from high HCHO columns on September 19, 2022. This independent analysis shows that recovered data can both improve the analysis of the HCHO:O_3 relationship and provide confidence in the scientific value of the new filtered dataset.

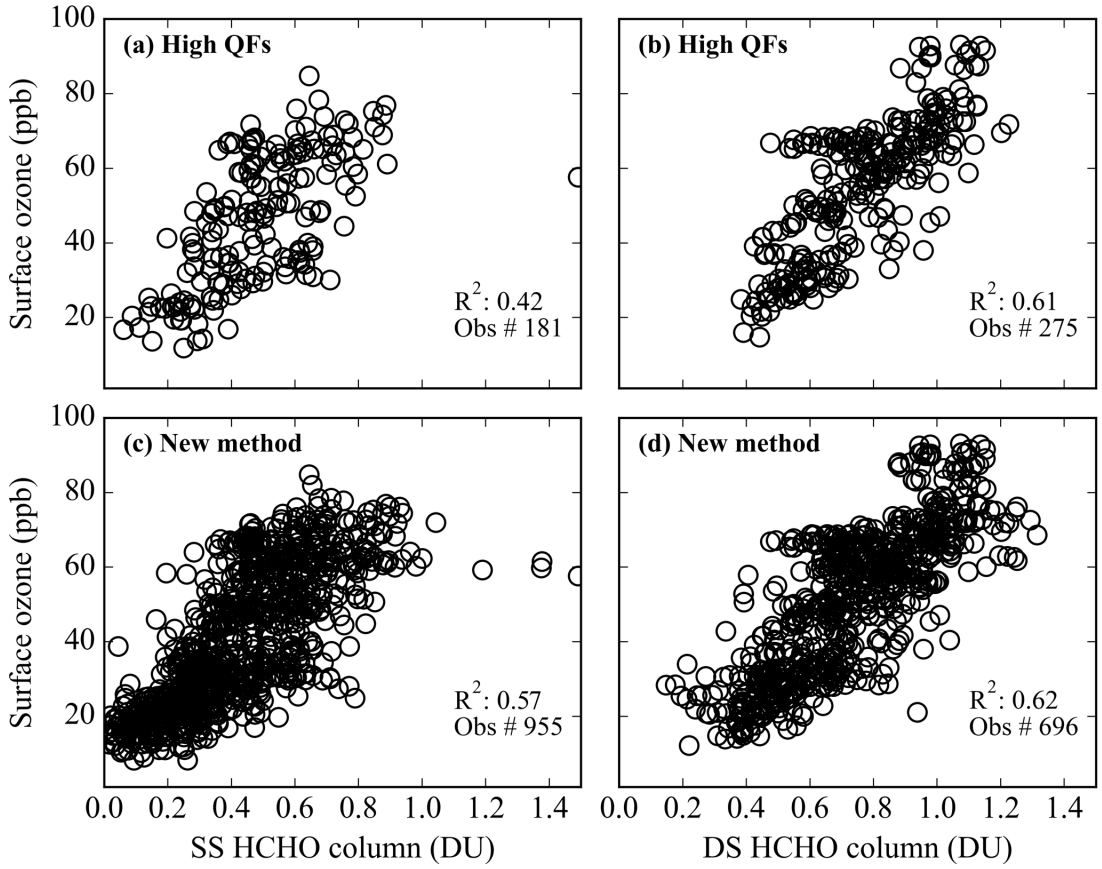

Figure 12. Relationship between Pandora HCHO column and surface ozone observations at the University of Houston site during TRACER-AQ in September 2021. Scatter plot between sky-scan HCHO column and surface ozone for (a) only high-quality flags and (c) data with new filtering method. Scatter plot between direct-sun HCHO column and surface ozone for (b) only high-quality flags and (d) data with new filtering method. HCHO column is given in Dobson units (1 DU= 2.69×10^{16} molecules cm^{-2}).

Table 1. Correlation (R^2) between hourly surface ozone and HCHO observations from direct-sun and sky-scan for high-quality data flags alone and for data using the new filtering method. Analysis is for four Pandora sites during September 2022. Each site is located near (within 500 m) an ozone monitoring instrument. The number (n) is the available hourly matchups for each site.

Site	Direct-sun		Sky-scan	
	High Quality Flags	New Filtering Method	High Quality Flags	New Filtering Method
Manhattan	R^2=0.36, n=59	R^2=0.43, n=156	R^2=0.62, n=152	R^2=0.64, n=164
Westport	R^2=0.47, n=99	R^2=0.55, n=165	R^2=0.56, n=115	R^2=0.57, n=189
New Brunswick	R^2=0.60, n=154	R^2=0.52, n=211	R^2=0.61, n=222	R^2=0.63, n=246
Bristol	R^2=0.71, n=109	R^2=0.67, n=209	R^2=0.74, n=183	R^2=0.72, n=241

3.2 Independent assessment of Pandora scientific data quality with airborne remote sensing

GEO-CAPE airborne simulator (GCAS) observations (Nowlan et al., 2018; Judd et al., 2020) provide an independent dataset of column NO_2 and HCHO observations to compare against Pandora over Houston, TX during the TRACER-AQ period (September 2021). Looking downward as it flies overhead at ~8.5 km, GCAS measures a partial column from the aircraft altitude down to the surface that includes the polluted boundary layer and a large portion of the less polluted free troposphere. Additionally, the GCAS tropospheric column measurements have been shown to strongly correlate with in-situ aircraft observations for NO_2 (R^2=0.89) and HCHO (R^2=0.54), with column differences in magnitude within 10% (Nowlan et al., 2018). Figure 13 shows the comparison of DS and SS observations with GCAS NO_2 and HCHO. To minimize the temporal and spatial mismatch between the Pandora and GCAS observations, GCAS was spatially filtered to include the nearest cloud-free GCAS pixels within 2.5 km of the Pandora location, and Pandora was temporally filtered to include observations in a 15-minute window centered on the time of the GCAS overpass.

Both the DS and SS NO_2 columns are well-correlated with GCAS (R^2 = 0.78 and 0.64, respectively). Some scatter can be attributed to GCAS uncertainties being on the order of 25% (Judd et al., 2020; Nawaz et al., 2024) from a priori uncertainties related to surface reflectivity and

trace gas profile. For DS NO_2 columns, there is a clear offset with Pandora columns exceeding GCAS values. The slope near unity and intercept of 3×10^{15} molecules cm^{-2} is consistent with the stratospheric amount that would be absent in the GCAS observations below the aircraft. Despite a few outliers (Figure 11b), there is no notable systematic bias between GCAS and SS NO_2. This is consistent with the SS NO_2 observations being limited to the most polluted lower few kilometers of the atmosphere. It could be argued that GCAS values tend to be slightly higher than SS observations of NO_2 due to the larger altitude range observed.

The correlations for GCAS and Pandora HCHO columns also show general agreement (R^2 = 0.50 and 0.51) but are weaker primarily due to the greater uncertainty in HCHO measurements for both instruments. For HCHO, the bias is in the SS rather than DS observations. This is due to the lack of significant HCHO in the free troposphere and stratosphere; thus, total columns associated with DS observations are more consistent with GCAS. Since HCHO is photochemically created, it tends to have a weaker vertical gradient in the polluted boundary layer compared to NO_2 which is much more weighted towards the surface where it is emitted. Thus, the limited altitude range of SS observations are more likely to miss some fraction of lower atmospheric HCHO and be biased low with respect to both DS and GCAS HCHO.

Overall, these comparisons are encouraging for both GCAS and Pandora with differences that are consistent with expectations based on the differences in DS and SS viewing sensitivities.

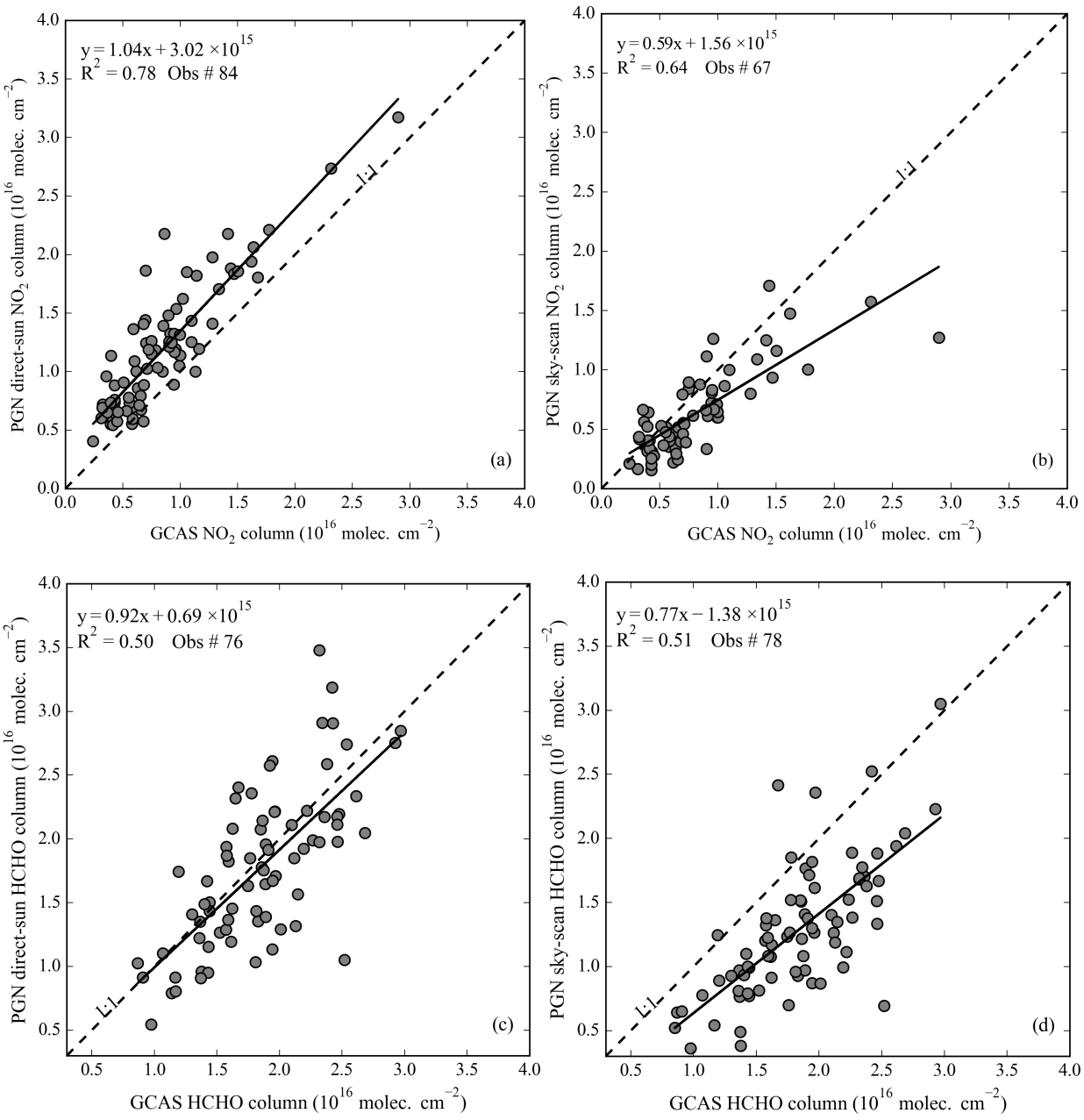

Figure 13. Comparison of airborne GCAS trace gas columns with and Pandora columns of NO_2 (panels a and b) and HCHO (panels c and d) during TRACER-AQ for Houston Pandora sites (Aldine, La Porte, and University of Houston). Comparisons are shown for both direct-sun (panels a and c) and sky-scan (panels b and d) modes.

3.3 Direct-sun and sky-scan intercomparison of column amounts

Given that the Pandora instrument spends significant time in both DS and SS modes, maximum data availability for scientific applications would be achieved by further addressing the causes of differences in their resulting measurements. DS and SS column measurements are expected to differ in their absolute amount due to limitations in the vertical sensitivity (for SS measurements), retrieval method (Herman et al., 2009; Frieß et al., 2019), and physical differences between tropospheric and stratospheric amounts. SS columns generally profile from the surface up to 2-4 km while DS columns observe the total column through the entire atmosphere. Due to its short lifetime and major secondary source from chemistry, the HCHO column has a weak gradient from the surface through the depth of the boundary layer (Schroeder et al., 2016; Crawford et al., 2021). This suggests that the DS HCHO total column should be greater than the SS lower tropospheric column, and the difference should be largely dependent on the vertical sensitivity of the SS measurement. For the NO_2 column, the stratospheric contribution is the largest influence on the differences between SS and DS column retrievals. To obtain a tropospheric DS NO_2 column, the NO_2 stratospheric column can be subtracted from the DS NO_2 total column using the stratospheric climatology provided by the PGN in their product based on Brohede et al. (2007).

Figure 14a shows the mean differences between the DS and SS column for HCHO and NO_2 over the 15 Pandora sites for 2021-2022. The bias for HCHO on average is 3.4×10^{15} molecules cm^{-2} with a larger bias at Hampton University in Virginia and New Haven, Connecticut ($>5 \times 10^{15}$ molecules cm^{-2}) and the smallest bias at Bayonne, New Jersey. The mean HCHO column in DS mode over these 15 sites averaged about 1×10^{16} molecules cm^{-2} making the bias between DS and SS mode approximately 35% of the column.

For NO_2, the mean difference was calculated after removing the stratospheric contribution (see red line in Figure 14a, Figure 14 is without removing stratospheric contribution). The remaining bias was less than 1×10^{15} or about 20% of the tropospheric column (5×10^{15}) on average. Higher average NO_2 columns ($>10\times10^{15}$ molecules cm^{-2}) were observed in New York (Manhattan, Bronx, and Queens) which also had three of the four highest biases observed. The highest bias was at Bayonne and appears to be anomalous, demonstrating that bias comparisons across the network are a useful tool for identifying potential problems at specific sites. In this case, Bayonne's large bias in NO_2

between SS and DS deserves a closer look by the site operator and may be related to a reference spectrum or calibration issue.

Figure 14 also shows how the bias between DS and SS for NO_2 (b) and HCHO (c) changes with solar zenith angle (SZA). One reason to expect changes in the bias with SZA is the larger uncertainty in AMF calculations and larger stray light contribution at high SZA (Herman et al., 2009). However, no consistent patterns in bias behavior versus SZA was found for either HCHO or NO_2. Pandoras at Aldine and the University of Houston showed increasing biases with increasing SZA for HCHO but the bias decreases with SZA at New Haven and Toronto and showed no variations with SZA for the New York Pandora instruments. The NO_2 column biases as a function of SZA showed no notable variation and were mostly constant around a mean value. Additionally, stray light is minimized in Pandora DS retrievals by subtracting the average signal below 290 nm from the spectra (Cede et al., ~~2021~~2024). However, residual stray light could contribute to large difference between DS and SS HCHO columns. Plotting the residual stray light as a function of SZA (Figure S1) showed that it decreased or remained constant (~ 0.3%) with increasing SZA, which suggests stray light contribution to the column might not increase significantly at higher SZA. There is also no evidence for a seasonal dependence in the difference between SS and DS observations (Figure S2 for the University of Houston), unlike that reported for the total ozone biases between Pandora and Brewer observations (Tzortziou et al., 2012).

Finally, the importance of differences in pointing azimuth and solar azimuth angle was investigated since 1) the Pandora SS analytical method may be less accurate when the solar azimuth and pointing azimuth are close (Cede et al., ~~2021~~2024), and 2) when the difference is large, the retrievals may be sampling different air masses. Figure S3 shows no systematic biases as a function of the difference between the pointing azimuth and solar azimuth across all 15 sites. This suggests that retrieval uncertainties and vertical sensitivity are most likely responsible for the mean biases between the SS and DS columns. This allows for the possibility of combining the two datasets for higher temporal coverage.

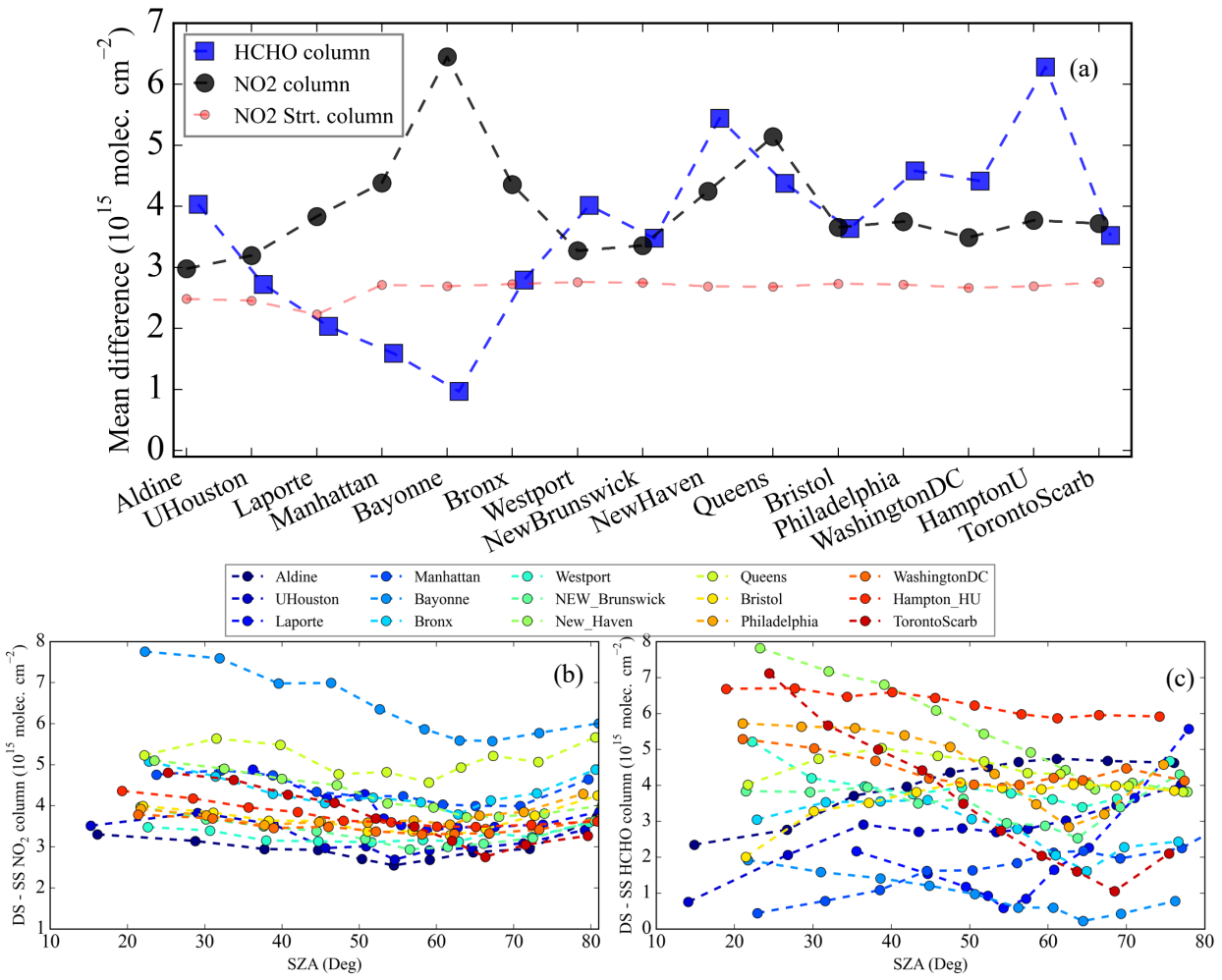

Figure 14. (a) Mean differences between the DS and SS column for HCHO and NO_2 over the 15 Pandora sites for 2021-2022. The NO_2 stratospheric column for each site is also provided. Bottom panels show the variation of mean column difference with SZA for NO_2 column (b) and HCHO columns (c), respectively.

3.4 Temporally combining DS and SS data

Section 2.2 discussed the standard schedule for Pandora observations with alternating measurements in the DS and SS modes and use of UV and open filters for the HCHO and NO_2 observations, respectively. The DS NO_2 retrieval is relatively fast compared to DS HCHO measurements which are less frequent. For SS measurements, both HCHO and NO_2 are comparable and take much longer than DS measurements (Figure 2c). In order to be combined, these time differences as well as biases diagnosed in the previous section must be addressed.

With the goal of creating a more continuous data record of hourly HCHO columns from Pandora suitable for comparison with hourly in situ measurements of surface ozone at EPA sites, Equation 1 combines data for DS and SS modes by correcting for the mean bias and then accounting for the difference in measurement times. Each column is weighted by the ratio between measurement time in each mode and total measurement time during the hour for both DS and SS modes. DS values for NO_2 column must first include subtraction of the stratospheric NO_2 contribution. SS observations are corrected by adding the mean bias value (Figure 14a). The summation of weighted values results in an hourly Pandora HCHO column.

$$X_{combined} = \sum_{i=1}^{1hr} X_{DS}[i] \times \frac{t_{eff}[i]}{Tot} + \sum_{j=1}^{1hr} \{X_{SS}[j] + MB\} \times \frac{\Delta t[j]}{Tot} \qquad \text{Eq. 1}$$

where t_{eff} is the effective measurement time for each DS observation (see column 3: "Effective duration of measurement" in the Pandora data files), Δt is the estimated measurement time for each SS observation (see Section S1.2 for details), Tot is the total integrated measurement time in a 1-hour period for both DS and SS measurements, $X_{DS}[i]$ is direct-sun column and $X_{SS}[j]$ is sky-scan column for the i^{th} and j^{th} measurements of each hour, respectively. MB is the mean bias of HCHO and NO_2 column between DS and SS measurements.

Table 2 shows the performance of the relationship between HCHO and hourly surface ozone at the University of Houston during September 2021 for SS, DS, and the combined dataset. The hourly correlation remains similar compared to high resolution data (5 min) as discussed in Figure 12, however the number of observations is lesser. The combined data set with new filtering method increased the temporal coverage of Pandora observations on the hourly data compared to using only one mode and high-quality flagged data. Applying the new filtering method to the combined data results in the greatest data coverage with better or equivalent correlation than for other subsets of data.

Table 2. Correlation (R^2) between hourly surface ozone and column HCHO from Sky-scan, Direct-sun, and combined data at the University of Houston site during TRACER-AQ (Sept 2021). Results include data with high quality only and with the new filtering method. The number of analyzed hours (n) is given for each case.

HCHO:O_3	High QFs	New filtering method
Sky-scan	R^2=0.41, n=132	R^2=0.61, n=234
Direct-sun	R^2=0.59, n=102	R^2=0.58, n=191
Combined data	R^2=0.50, n=162	R^2=0.62, n=240

4 Summary and conclusions

The growing Pandonia Global Network of Pandora spectrometers provides a ground-based network of remote sensing observations to both validate satellite trace gas retrievals and understand local air quality. Pandora provides information on the diurnal variability of multiple species (e.g., NO_2 and HCHO) using two independent viewing geometries: direct-sun (DS) and sky-scan (SS) modes. The Pandora quality assurance procedure recommends using high-quality flagged data, exercising caution with medium-quality flagged data, and not using low-quality flagged data. Unfortunately, high quality data can often be only a small fraction of the total set of observations, except for DS NO_2 columns.

In response to the overly stringent data flagging procedure, a framework has been described for analyzing Pandora observations by taking advantage of the two independent modes of operation. This ~~work presents~~includes a new filtering method ~~developed and tested~~ as an alternative to using quality flags to identify scientifically useful observations. The need to filter data is not new as Pandora users selected filtering criteria with some level of subjectivity in years prior to development of the PGN quality flagging procedure (Herman et al., 2009; Judd et al., 2019; Tzortziou et al., 2022).

The method keys on the range of independent uncertainty values for Pandora data flagged as high quality. Given the large overlap in independent uncertainty for high-, medium-, and low-quality

flagged data, the μ+3σ value of independent uncertainty for the high-quality flagged data defines a cut-off that preserves almost all high-quality data and includes a large amount of medium- and low-quality flagged data. A final step in the method is to restore observations with a percent uncertainty of less than 10%. For a much smaller number of data, wrms > 0.01 (normalized root mean square of the fitting residuals weighted with the independent uncertainty) and SS MHzD > 20 km (maximum horizontal distance) should also be filtered out.

Given the independence and contemporaneous nature of DS and SS observation modes, correlation of adjacent (within 5 min) observations between modes provides evidence for scientifically useful data in the medium- and low-quality flagged data. Unfiltered observations already exhibit some degree of correlation for data with medium- and low-quality flags, but for filtered data, quality flags appear to have no influence on correlations for various pairing of DS and SS quality flags. This is particularly important in that the method can recover as much as 90% of data that would have previously been discarded. Further analysis suggests that the standard PGN data flags for atmospheric variability and wrms are too stringent based on the quality of data recovered that exceed PGN criteria for those values.

The strong relationship between column HCHO and surface ozone provided a method for testing the new filtering method. At the University of Houston and four additional sites with nearby ozone monitors, filtered data resulted in a similar or improved relationship between column HCHO and surface ozone with 14-63% more data than using high quality data alone.

Airborne GCAS observations from the TRACER-AQ campaign in Houston provided an independent set of NO_2 and HCHO column observations to compare against filtered Pandora DS and SS observations. The two datasets correlated well, but biases were also observed related to differences in the total column DS observations versus SS observations that have sensitivity limited to the lowest 2-4 km of the atmosphere.

Combining SS and DS data provided better hourly data coverage after correcting for biases between the two modes. Across 15 Pandora sites in the domain of recent NASA field campaigns, the HCHO column biases ranged from 0.8×10^{15} molecules cm^{-2} to 6×10^{15} molecules cm^{-2} (8 to 60% of the average column of 1×10^{16} molecules cm^{-2}). The NO_2 tropospheric column biases were

less than 1×10^{15} molecules cm^{-2} (20% of the average column of 0.5×10^{16} molecules cm^{-2} except for at the Bayonne, NJ Pandora). The biases in NO_2 and HCHO between DS and SS observations were examined for trends with solar zenith angle (SZA), viewing azimuth angle, and residual stray light. No systematic behavior in the biases were found.

A more continuous hourly Pandora dataset was constructed for comparison with hourly surface ozone. This dataset required correcting the site-specific biases in DS and SS observations as well as weighting the observations based on their different measurement durations. The combined hourly dataset showed similar or improved correlations with surface ozone with a 30-40% increase in hourly data coverage.

The proposed filtering method and improved representation of hourly average conditions by combining DS and SS data offer the community useful strategies for using Pandora observations to their fullest potential for validating geostationary satellite observations and informing local air quality.

Data availability. The Pandora data is available at PGN website (https://www.pandonia-global-network.org). The airborne GCAS observation during TRACER-AQ period can be obtained from https://www-air.larc.nasa.gov/cgi-bin/ArcView/traceraq.2021. Surface ozone data at hourly and 5-minutes resolution is obtained from the EPA (https://www.epa.gov/ground-level-ozone-pollution) and ARM-TRACER-AQ (https://adc.arm.gov/discovery/#/results/s::tracer%20tceq) website, respectively.

Author contributions. PR, JHC, and KRT designed the study and PR performed the data analysis. PR and KRT interpreted the results and wrote the initial draft of the paper. LJ, JHC, KRT, JS, LV, MAGD, AW, EB and TFH provided significant conceptual input to the design of the manuscript and the improvement of the manuscript. All authors discussed the results and analysis.

Competing interests. At least one of the (co-)authors is a member of the editorial board of Atmospheric Measurement Techniques.

Acknowledgements. We thank the PI(s), support staff and funding for establishing and maintaining the 15 Pandora sites of the PGN used in this investigation, specifically we thank Jimmy Flynn, Maria Tzortziou, Nader Abuhassan, John Anderson, and Vitali Fioletov. We thank the ESA and

NASA joint PGN for Pandora data processing and data disseminations. We thank NASA GFSC for Pandora calibration, in particular Apoorva Pandey and Bryan Place. NASA Postdoctoral Program at the NASA Langley Research Center, administered by ORAU under contract with NASA acknowledged for funding PR. LMJ and KRT acknowledge NASA grant 80NSSC24M0094. We acknowledge the GCAS groups for the TRACER-AQ 2021 filed campaign datasets. We thank EPA and TCEQ for surface ozone observations.

***Disclaimer*:** The research described in this article has been reviewed by the U.S. Environmental Protection Agency (EPA) and approved for publication. Approval does not signify that the contents necessarily reflect the views and the policies of the agency nor does mention of trade names or commercial products constitute endorsement or recommendation for use.

References:

Adams, T. J., Geddes, J. A., and Lind, E. S.: New Insights Into the Role of Atmospheric Transport and Mixing on Column and Surface Concentrations of NO_2 at a Coastal Urban Site, JGR Atmospheres, 128, e2022JD038237, https://doi.org/10.1029/2022JD038237, 2023.

Brohede, S. M., Haley, C. S., McLinden, C. A., Sioris, C. E., Murtagh, D. P., Petelina, S. V., Llewellyn, E. J., Bazureau, A., Goutail, F., Randall, C. E., Lumpe, J. D., Taha, G., Thomasson, L. W., and Gordley, L. L.: Validation of Odin/OSIRIS stratospheric NO_2 profiles, J. Geophys. Res., 112, 2006JD007586, https://doi.org/10.1029/2006JD007586, 2007.

Cede, A., Herman, J., Richter, A., Krotkov, N., and Burrows, J.: Measurements of nitrogen dioxide total column amounts using a Brewer double spectrophotometer in direct Sun mode, Journal of Geophysical Research: Atmospheres, 111, https://doi.org/10.1029/2005JD006585, 2006.

Cede, A~~., Tiefengraber, M., Gebetsberger, M., and Kreuter, M~~.: TN on Manual for Blick Software Suite manual version 1.8-5, Pandonia Global Network, available at: https://www.pandonia-global-network.org/wp-content/uploads/~~2021/09/BlickSoftwareSuit~~2024/08/BlickSoftwareSuite_Manual_v1-8-~~4~~5.pdf (last access: 27 ~~Sep 2023), 2021~~Feb 2025), 2024.

Cede, A., Santana, D., Tiefengraber, M., Muller, M., and Gebetsberger, M.: on Fiducial Reference Measurements for Air Quality, TN on change/upgrade of instrument, Pandonia Global Network, available at: https://www.~~pandoniaglobalnetwork~~pandonia-global-network.org/~~wpcontent~~wp-

content/uploads/2022/12/LuftBlick_FRM4AQ_InstrumentChangeUpgrade_RP_2019002_v8.pdf (last access: 27 Sep ~~2023~~2024), 2022.

~~Cede, A., Tiefengraber, M., Gebetsberger, M., and Lind E.: TN on on Pandonia Global Network Data Products Readme Document version 1.8-8, https://www.pandonia-global-network.org/wp-content/uploads/2023/11/PGN_DataProducts_Readme_v1-8-8.pdf (last access: 27 Sep 2023), 2023a.~~

Cede, A., Tiefengraber, M., Gebetsberger, M., and Lind E.: TN on on Pandonia Global Network Data Products Readme Document version 1.8-~~7, Pandonia Global Network, available at:~~8, https://www.~~pandoniaglobalnetwork~~pandonia-global-network.org/~~wpcontent~~wp-content/uploads/~~2023/08~~2025/01/PGN_DataProducts_Readme_v1-8-~~7~~10.pdf (last access: ~~27 Sep 2023), 2023b~~20 Mar 2025), 2025.

Chang, L.-S., Kim, D., Hong, H., Kim, D.-R., Yu, J.-A., Lee, K., Lee, H., Kim, D., Hong, J., Jo, H.-Y., and Kim, C.-H.: Evaluation of correlated Pandora column NO $_2$ and in situ surface NO $_2$ measurements during GMAP campaign, Atmos. Chem. Phys., 22, 10703–10720, https://doi.org/10.5194/acp-22-10703-2022, 2022.

Choi, S., Lamsal, L. N., Follette-Cook, M., Joiner, J., Krotkov, N. A., Swartz, W. H., Pickering, K. E., Loughner, C. P., Appel, W., Pfister, G., Saide, P. E., Cohen, R. C., Weinheimer, A. J., and Herman, J. R.: Assessment of NO2 observations during DISCOVER-AQ and KORUS-AQ field campaigns, Atmos. Meas. Tech., 13, 2523–2546, https://doi.org/10.5194/amt-13-2523-2020, 2020.

Crawford, J.H., Ahn, J.Y., Al-Saadi, J., Chang, L., Emmons, L.K., Kim, J., Lee, G., Park, J.H., Park, R.J., Woo, J.H. and Song, C.K., The Korea–United States air quality (KORUS-AQ) field study. *Elem Sci Anth*, *9*(1), p.00163, 2021.

Di Bernardino, A., Mevi, G., Iannarelli, A. M., Falasca, S., Cede, A., Tiefengraber, M., and Casadio, S.: Temporal Variation of NO2 and O3 in Rome (Italy) from Pandora and In Situ Measurements, Atmosphere, 14, 594, https://doi.org/10.3390/atmos14030594, 2023.

Frieß, U., Beirle, S., Alvarado Bonilla, L., Bösch, T., Friedrich, M. M., Hendrick, F., Piters, A., Richter, A., Van Roozendael, M., Rozanov, V. V., Spinei, E., Tirpitz, J.-L., Vlemmix, T., Wagner, T., and Wang, Y.: Intercomparison of MAX-DOAS vertical profile retrieval algorithms: studies using synthetic data, Atmos. Meas. Tech., 12, 2155–2181, https://doi.org/10.5194/amt-12-2155-2019, 2019.

Gebetsberger, M., ~~and Tiefengraber, M.: on Evolution of QA/QC Strategies, Pandonia Global Network, available at https://www.pandoniaglobalnetwork.org/wpcontent/uploads/2023/08/PGN_DataProducts_Readme_v1-8-7.pdf (last access: 27 Sep 2023), 2023a.~~

~~Gebetsberger, M., ~~Tiefengraber, M., Cede, A.: Fiducial Reference Measurements for Air Quality, TN on Data Quality Flagging Generic Procedure Evolution, Pandonia Global Network, available

at: https://www.pandoniaglobalnetworkpandonia-global-network.org/wpcontent/uploads/2023/08/PGN_DataProducts_Readme_v1-8-7wp-content/uploads/2023/01/LuftBlick_FRM4AQ_DataQualityFlaggingGenericProcedureEvolution_TN_2019008_v7.pdf (last access: 27 Sep 2023), 2023b.2022.

Gebetsberger, M., and Tiefengraber, M.: on Evolution of QA/QC Strategies, Pandonia Global Network, available at https://www.pandonia-global-network.org/wp-content/uploads/2023/08/LuftBlick_FRM4AQ-2_Evolution-Of-QAQC-Strategies_TN_2023008_v1.pdf (last access: 27 Sep 2023), 2023.

Goldberg, D. L., Lamsal, L. N., Loughner, C. P., Swartz, W. H., Lu, Z., and Streets, D. G.: A high-resolution and observationally constrained OMI NO₂ NO_2 satellite retrieval, Atmos. Chem. Phys., 17, 11403–11421, https://doi.org/10.5194/acp-17-11403-2017, 2017.

Herman, J., Cede, A., Spinei, E., Mount, G., Tzortziou, M., and Abuhassan, N.: NO_2 column amounts from ground- based Pandora and MFDOAS spectrometers using the direct-sun DOAS technique: Intercomparisons and appli- cation to OMI validation, J. Geophys. Res., 114, D13307, https://doi.org/10.1029/2009JD011848, 2009.

Herman, J., Spinei, E., Fried, A., Kim, J., Kim, J., Kim, W., Cede, A., Abuhassan, N., and Segal-Rozenhaimer, M.: NO_2 and HCHO measurements in Korea from 2012 to 2016 from Pandora spec trometer instruments compared with OMI retrievals and with aircraft measurements during the KORUS-AQ campaign, At- mos. Meas. Tech., 11, 4583–4603, https://doi.org/10.5194/amt- 11-4583-2018, 2018.

Herman, J., Abuhassan, N., Kim, J., Kim, J., Dubey, M., Raponi, M., and Tzortziou, M.: Underestimation of column NO2 amounts from the OMI satellite compared to diurnally varying ground-based retrievals from multiple PANDORA spectrometer instruments, Atmos. Meas. Tech., 12, 5593–5612, https://doi.org/10.5194/amt-12-5593-2019, 2019.

Ialongo, I., Virta, H., Eskes, H., Hovila, J., and Douros, J.: Comparison of TROPOMI/Sentinel-5 Precursor NO2 observations with ground-based measurements in Helsinki, Atmos. Meas. Tech., 13, 205–218, https://doi.org/10.5194/amt-13-205-2020, 2020.

Judd, L. M., Al-Saadi, J. A., Valin, L. C., Pierce, R. B., Yang, K., Janz, S. J., Kowalewski, M. G., Szykman, J. J., Tiefengraber, M., and Mueller, M.: The Dawn of Geostationary Air Quality Monitoring: Case Studies From Seoul and Los Angeles, Front. Environ. Sci., 6, 85, https://doi.org/10.3389/fenvs.2018.00085, 2018.

Judd, L. M., Al-Saadi, J. A., Janz, S. J., Kowalewski, M. G., Pierce, R. B., Szykman, J. J., Valin, L. C., Swap, R., Cede, A., Mueller, M., Tiefengraber, M., Abuhassan, N., and Williams, D.: Evaluating the impact of spatial resolution on tropospheric NO_2 column comparisons within urban areas using high-resolution airborne data, Atmos. Meas. Tech., 12, 6091–6111, https://doi.org/10.5194/amt-12-6091-2019, 2019.

Judd, L. M., Al-Saadi, J. A., Szykman, J. J., Valin, L. C., Janz, S. J., Kowalewski, M. G., Eskes, H. J., Veefkind, J. P., Cede, A., Mueller, M., Gebetsberger, M., Swap, R., Pierce, R. B., Nowlan, C. R., Abad, G. G., Nehrir, A., and Williams, D.: Evaluating Sentinel-5P TROPOMI tropospheric NO2 column densities with airborne and Pandora spectrometers near New York City and Long Island Sound, Atmos. Meas. Tech., 13, 6113–6140, https://doi.org/10.5194/amt-13-6113-2020, 2020.

Kim, J., Kim, M., and Choi, M.: Monitoring aerosol properties in east asia from geostationary orbit: GOCI, MI and GEMS, in Air Pollution in Eastern Asia: An Integrated Perspective ISSI Scientific Report Series. (Cham: Springer), 323–333, 2017.

Kim, S., Kim, D., Hong, H., Chang, L.-S., Lee, H., Kim, D.-R., Kim, D., Yu, J.-A., Lee, D., Jeong, U., Song, C.-K., Kim, S.-W., Park, S. S., Kim, J., Hanisco, T. F., Park, J., Choi, W., and Lee, K.: First-time comparison between NO_2 vertical columns from Geostationary Environmental Monitoring Spectrometer (GEMS) and Pandora measurements, Atmos. Meas. Tech., 16, 3959–3972, https://doi.org/10.5194/amt-16-3959-2023, 2023.

Liu, O., Li, Z., Lin, Y., Fan, C., Zhang, Y., Li, K., Zhang, P., Wei, Y., Chen, T., Dong, J., and De Leeuw, G.: Evaluation of the first year of Pandora NO_2 measurements over Beijing and application to satellite validation, Gases/Remote Sensing/Validation and Intercomparisons, https://doi.org/10.5194/amt-2023-177, 2023.

Nawaz, M. O., Johnson, J., Yarwood, G., de Foy, B., Judd, L., and Goldberg, D. L.: An intercomparison of satellite, airborne, and ground-level observations with WRF–CAMx simulations of NO_2 columns over Houston, Texas, during the September 2021 TRACER-AQ campaign, Atmos. Chem. Phys., 24, 6719–6741, https://doi.org/10.5194/acp-24-6719-2024, 2024.

Nowlan, C. R., Liu, X., Janz, S. J., Kowalewski, M. G., Chance, K., Follette-Cook, M. B., Fried, A., González Abad, G., Herman, J. R., Judd, L. M., Kwon, H.-A., Loughner, C. P., Pickering, K. E., Richter, D., Spinei, E., Walega, J., Weibring, P., and Weinheimer, A. J.: Nitrogen dioxide and formaldehyde measurements from the GEOstationary Coastal and Air Pollution Events (GEO-CAPE) Airborne Simulator over Houston, Texas, Atmos. Meas. Tech., 11, 5941–5964, https://doi.org/10.5194/amt-11-5941-2018, 2018.

Park, J.-U., Park, J.-S., Diaz, D. S., Gebetsberger, M., Müller, M., Shalaby, L., Tiefengraber, M., Kim, H.-J., Park, S. S., Song, C.-K., and Kim, S.-W.: Spatiotemporal inhomogeneity of total column NO_2 in a polluted urban area inferred from TROPOMI and Pandora intercomparisons, GIScience & Remote Sensing, 59, 354–373, https://doi.org/10.1080/15481603.2022.2026640, 2022.

Reed, A. J., Thompson, A. M., Kollonige, D. E., Martins, D. K., Tzortziou, M. A., Herman, J. R., Berkoff, T. A., Abuhassan, N. K., and Cede, A.: Effects of local meteorology and aerosols on ozone and nitrogen dioxide retrievals from OMI and pandora spectrometers in Maryland, USA during DISCOVER-AQ 2011, J Atmos Chem, 72, 455–482, https://doi.org/10.1007/s10874-013-9254-9, 2015.

Schroeder, J. R., Crawford, J. H., Fried, A., Walega, J., Weinheimer, A., Wisthaler, A., Müller, M., Mikoviny, T., Chen, G., Shook, M., Blake, D. R., Diskin, G., Estes, M., Thompson, A. M., Lefer, B. L., Long, R., and Mattson, E.: Formaldehyde column density measurements as a suitable pathway to estimate near-surface ozone tendencies from space, J. Geophys. Res. Atmos., 121, 13,088-13,112, https://doi.org/10.1002/2016JD025419, 2016.

Spinei, E., Whitehill, A., Fried, A., Tiefengraber, M., Knepp, T. N., Herndon, S., Herman, J. R., Müller, M., Abuhassan, N., Cede, A., Richter, D., Walega, J., Crawford, J., Szykman, J., Valin, L., Williams, D. J., Long, R., Swap, R. J., Lee, Y., Nowak, N., and Poche, B.: The first evaluation of formaldehyde column observations by improved Pandora spectrometers during the KORUS-AQ field study, Atmos. Meas. Tech., 11, 4943–4961, https://doi.org/10.5194/amt-11-4943-2018, 2018.

Spinei, E., Tiefengraber, M., Müller, M., Gebetsberger, M., Cede, A., Valin, L., Szykman, J., Whitehill, A., Kotsakis, A., Santos, F., Abbuhasan, N., Zhao, X., Fioletov, V., Lee, S. C., and Swap, R.: Effect of polyoxymethylene (POM-H Delrin) off-gassing within the Pandora head sensor on direct-sun and multi-axis formaldehyde column measurements in 2016–2019, Atmos. Meas. Tech., 14, 647–663, https://doi.org/10.5194/amt-14-647-2021, 2021.

Szykman, J., Swap, R., Leffer, B., Valin, L., Lee, S. C., Fioletov, V., Zhao, X., Davis, J., Williams, D., Abuhassan, N., Shalaby, L., Cede, A., Tiefengraber, M., Müller, M., Kotsakis, A., San- tos, F., and Robinson, J.: Connecting in-situ and Satellite Mon- itoring in Support of the Canada – U.S. Air Quality Agree- ment, Environmental Managers magazine, Air & Waste Man- agement Association, 1–7, available at: https://www.awma.org/~~flip/EM-June-2019/szykman.pdf~~emjune19 (last access: 27 Sep 2023), 2019.

Szykman, J. J. and Liu, X.: Level 2 Science Data Product Validation Plan, 2023.

Tirpitz, J.-L., Frieß, U., Hendrick, F., Alberti, C., Allaart, M., Apituley, A., Bais, A., Beirle, S., Berkhout, S., Bognar, K., Bösch, T., Bruchkouski, I., Cede, A., Chan, K. L., Den Hoed, M., Donner, S., Drosoglou, T., Fayt, C., Friedrich, M. M., Frumau, A., Gast, L., Gielen, C., Gomez-Martín, L., Hao, N., Hensen, A., Henzing, B., Hermans, C., Jin, J., Kreher, K., Kuhn, J., Lampel, J., Li, A., Liu, C., Liu, H., Ma, J., Merlaud, A., Peters, E., Pinardi, G., Piters, A., Platt, U., Puentedura, O., Richter, A., Schmitt, S., Spinei, E., Stein Zweers, D., Strong, K., Swart, D., Tack, F., Tiefengraber, M., Van Der Hoff, R., Van Roozendael, M., Vlemmix, T., Vonk, J., Wagner, T., Wang, Y., Wang, Z., Wenig, M., Wiegner, M., Wittrock, F., Xie, P., Xing, C., Xu, J., Yela, M., Zhang, C., and Zhao, X.: Intercomparison of MAX-DOAS vertical profile retrieval algorithms: studies on field data from the CINDI-2 campaign, Atmos. Meas. Tech., 14, 1–35, https://doi.org/10.5194/amt-14-1-2021, 2021.

Travis, K. R., Judd, L. M., Crawford, J. H., Chen, G., Szykman, J., Whitehill, A., Valin, L. C., Spinei, E., Janz, S., Nowlan, C. R., Kwon, H., Fried, A., and Walega, J.: Can Column Formaldehyde Observations Inform Air Quality Monitoring Strategies for Ozone and Related Photochemical Oxidants?, JGR Atmospheres, 127, https://doi.org/10.1029/2022JD036638, 2022.

Tzortziou, M., Herman, J. R., Cede, A., and Abuhassan, N.: High precision, absolute total column ozone measurements from the Pandora spectrometer system: Comparisons with data from a Brewer double monochromator and Aura OMI, J. Geophys. Res., 117, 2012JD017814, https://doi.org/10.1029/2012JD017814, 2012.

Tzortziou, M., Kwong, C. F., Goldberg, D., Schiferl, L., Commane, R., Abuhassan, N., Szykman, J. J., and Valin, L. C.: Declines and peaks in NO_2 pollution during the multiple waves of the COVID-19 pandemic in the New York metropolitan area, Atmos. Chem. Phys., 22, 2399–2417, https://doi.org/10.5194/acp-22-2399-2022, 2022.

Tzortziou, M., Loughner, C. P., Goldberg, D. L., Judd, L., Nauth, D., Kwong, C. F., Lin, T., Cede, A., and Abuhassan, N.: Intimately tracking NO2 pollution over the New York City - Long Island Sound land-water continuum: An integration of shipboard, airborne, satellite observations, and models, Science of The Total Environment, 897, 165144, https://doi.org/10.1016/j.scitotenv.2023.165144, 2023.

Veefkind, J. P., Aben, I., McMullan, K., Förster, H., De Vries, J., Otter, G., Claas, J., Eskes, H. J., De Haan, J. F., Kleipool, Q., Van Weele, M., Hasekamp, O., Hoogeveen, R., Landgraf, J., Snel, R., Tol, P., Ingmann, P., Voors, R., Kruizinga, B., Vink, R., Visser, H., and Levelt, P. F.: TROPOMI on the ESA Sentinel-5 Precursor: A GMES mission for global observations of the atmospheric composition for climate, air quality and ozone layer applications, Remote Sensing of Environment, 120, 70–83, https://doi.org/10.1016/j.rse.2011.09.027, 2012.

Verhoelst, T., Compernolle, S., Pinardi, G., Lambert, J.-C., Eskes, H. J., Eichmann, K.-U., Fjæraa, A. M., Granville, J., Niemeijer, S., Cede, A., Tiefengraber, M., Hendrick, F., Pazmiño, A., Bais, A., Bazureau, A., Boersma, K. F., Bognar, K., Dehn, A., Donner, S., Elokhov, A., Gebetsberger, M., Goutail, F., Grutter De La Mora, M., Gruzdev, A., Gratsea, M., Hansen, G. H., Irie, H., Jepsen, N., Kanaya, Y., Karagkiozidis, D., Kivi, R., Kreher, K., Levelt, P. F., Liu, C., Müller, M., Navarro Comas, M., Piters, A. J. M., Pommereau, J.-P., Portafaix, T., Prados-Roman, C., Puentedura, O., Querel, R., Remmers, J., Richter, A., Rimmer, J., Rivera Cárdenas, C., Saavedra De Miguel, L., Sinyakov, V. P., Stremme, W., Strong, K., Van Roozendael, M., Veefkind, J. P., Wagner, T., Wittrock, F., Yela González, M., and Zehner, C.: Ground-based validation of the Copernicus Sentinel-5P TROPOMI NO2 measurements with the NDACC ZSL-DOAS, MAX-DOAS and Pandonia global networks, Atmos. Meas. Tech., 14, 481–510, https://doi.org/10.5194/amt-14-481-2021, 2021.

Vigouroux, C., Langerock, B., Bauer Aquino, C. A., Blumenstock, T., Cheng, Z., De Mazière, M., De Smedt, I., Grutter, M., Hannigan, J. W., Jones, N., Kivi, R., Loyola, D., Lutsch, E., Mahieu, E., Makarova, M., Metzger, J.-M., Morino, I., Murata, I., Nagahama, T., Notholt, J., Ortega, I., Palm, M., Pinardi, G., Röhling, A., Smale, D., Stremme, W., Strong, K., Sussmann, R., Té, Y., Van Roozendael, M., Wang, P., and Winkler, H.: TROPOMI–Sentinel-5 Precursor formaldehyde validation using an extensive network of ground-based Fourier-transform infrared stations, Atmos. Meas. Tech., 13, 3751–3767, https://doi.org/10.5194/amt-13-3751-2020, 2020.

Wang, S., Pongetti, T. J., Sander, S. P., Spinei, E., Mount, G. H., Cede, A., & Herman, J.: Direct Sun Measurements of NO_2 column abundances from Table Mountain, California: Intercomparison

of low-and high-resolution spectrometers. Journal of Geophysical Research, Atmosphere 115, D13305. https://doi.org/10.1029/2009JD013503, 2010.

Wang, B., Geddes, J. A., Adams, T. J., Lind, E. S., McDonald, B. C., He, J., Harkins, C., Li, D., and Pfister, G. G.: Implications of Sea Breezes on Air Quality Monitoring in a Coastal Urban Environment: Evidence From High Resolution Modeling of NO2 and O3, Journal of Geophysical Research: Atmospheres, 128, e2022JD037860, https://doi.org/10.1029/2022JD037860, 2023.

Yang, L. H., Jacob, D. J., Colombi, N. K., Zhai, S., Bates, K. H., Shah, V., Beaudry, E., Yantosca, R. M., Lin, H., Brewer, J. F., Chong, H., Travis, K. R., Crawford, J. H., Lamsal, L. N., Koo, J.-H., and Kim, J.: Tropospheric NO_2 vertical profiles over South Korea and their relation to oxidant chemistry: implications for geostationary satellite retrievals and the observation of NO_2 diurnal variation from space, Atmos. Chem. Phys., 23, 2465–2481, https://doi.org/10.5194/acp-23-2465-2023, 2023.

Zoogman, P., Liu, X., Suleiman, R. M., Pennington, W. F., Flittner, D. E., Al-Saadi, J. A., Hilton, B. B., Nicks, D. K., Newchurch, M. J., Carr, J. L., Janz, S. J., Andraschko, M. R., Arola, A., Baker, B. D., Canova, B. P., Chan Miller, C., Cohen, R. C., Davis, J. E., Dussault, M. E., Edwards, D. P., Fishman, J., Ghulam, A., González Abad, G., Grutter, M., Herman, J. R., Houck, J., Jacob, D. J., Joiner, J., Kerridge, B. J., Kim, J., Krotkov, N. A., Lamsal, L., Li, C., Lindfors, A., Martin, R. V., McElroy, C. T., McLinden, C., Natraj, V., Neil, D. O., Nowlan, C. R., O′Sullivan, E. J., Palmer, P. I., Pierce, R. B., Pippin, M. R., Saiz-Lopez, A., Spurr, R. J. D., Szykman, J. J., Torres, O., Veefkind, J. P., Veihelmann, B., Wang, H., Wang, J., and Chance, K.: Tropospheric emissions: Monitoring of pollution (TEMPO), Journal of Quantitative Spectroscopy and Radiative Transfer, 186, 17–39, https://doi.org/10.1016/j.jqsrt.2016.05.008, 2017.